



รายงานวิจัยฉบับสมบูรณ์

โครงการ Development of SERS based biosensors for cancer screening

โดย นางสาวสุวัสสา บำรุงทรัพย์

25 กันยายน พ.ศ. 2562

สัญญาเลขที่ TRG6080003

รายงานวิจัยฉบับสมบูรณ์

โครงการ Development of SERS based biosensors for cancer screening

ผู้วิจัย นางสาวสุวัสสา บำรุงทรัพย์ สังกัด ศูนย์นาโนเทคโนยีแห่งชาติ

สนับสนุนโดยสำนักงานกองทุนสนับสนุนการวิจัยและ ต้นสังกัด

(ความเห็นในรายงานนี้เป็นของผู้วิจัย สกว.และต้นสังกัดไม่จำเป็นต้องเห็นด้วยเสมอไป)

รูปแบบ Abstract (บทคัดย่อ)

Project Code: TRG6080003

(รหัสโครงการ)

Project Title : Development of SERS based biosensors for cancer screening (ชื่อโครงการ)

Investigator : ผู้วิจัย นางสาวสุวัสสา บำรุงทรัพย์ สังกัด ศูนย์นาโนเทคโนยีแห่งชาติ (ชื่อนักวิจัย)

E-mail Address: suwussa@nanotec.or.th

Project Period : 3 เมษายน 2560 – 2 เมษายน 2562 (ระยะเวลาโครงการ)

เนื้อหางานวิจัยประกอบด้วย วัตถุประสงค์ วิธีทดลอง ผลการทดลอง สรุปและวิจารณ์ผล การทดลอง และข้อเสนอแนะสำหรับงานวิจัยในอนาคต

Keywords : Surface enhanced Raman scattering (SERS), plasmonic paper, gold nanorod, biosensor, miRNA (คำหลัก)

Output จากโครงการวิจัยที่ได้รับทุนจาก สกว.

- 1. ผลงานตีพิมพ์ในวารสารวิชาการนานาชาติ (ระบุชื่อผู้แต่ง ชื่อเรื่อง ชื่อวารสาร ปี เล่มที่ เลขที่ และหน้า) หรือผลงานตามที่คาดไว้ในสัญญาโครงการ
- 1.1 Reokrungruang P, Chatnuntawech I, Dharakul T, <u>Bamrungsap S*</u> (2019) A simple paper-based surface enhanced Raman scattering (SERS) platform and magnetic separation for cancer screening. Sensors & Actuator B, 285, 462-469. (IF=6.393)
- 1.2 Treerattrakoon K, Polamuangdee K, Dharakul T, <u>Bamrungsap S*</u> Development of SERS tag for microRNA detection (submitted)
 - 2. การนำผลงานวิจัยไปใช้ประโยชน์

ประโยชน์เชิงวิชาการโดยการสร้างองค์ความรู้ใหม่ในการพัฒนาไบโอเซ็นเซอร์ที่ใช้หลักการ ขยายสัญญาณรามาน (SERS) สำหรับตรวจคัดกรองมะเร็ง โดยมีการยื่นจดอนุสิทธิบัตรจำนวน 2 ฉบับ ตีพิมพ์ในวารสารนานาชาติจำนวน 1 ฉบับ และกำลังยื่นส่งตีพิมพ์ในวารสารนานาชาติ อีก 1 ฉบับ

- 3. อื่นๆ (เช่น ผลงานตีพิมพ์ในวารสารวิชาการในประเทศ การเสนอผลงานในที่ประชุม วิชาการ หนังสือ การจดสิทธิบัตร)
- 3.1 ยื่นจดอนุสิทธิบัตรเรื่อง "ชุดตรวจวัดสัญญาณการกระเจิงแสงรามานของเซลล์มะเร็ง" กันยายน 2561
- 3.2 ยื่นจดอนุสิทธิบัตรเรื่อง "น้ำยาสำหรับตรวจหาไมโครอาร์เอ็นเอ" กันยายน 2562
- 3.3 The 1st MRS-Thailand Conference 2017, Chiangmai, Thailand (Poster presentation award)
- 3.4 Applied Nanotechnology and Nanoscience International Conference (ANNIC)2018, Berlin, Germany (Oral presentation)
 - 3.5 The 2nd MRS-Thailand Conference 2019, Pattaya, Thailand (Oral presentation)

Project title: "Development of SERS based biosensors for cancer screening"

Project duration: 2 years

Total budget: 600,000 Baht

Principal investigator: Suwussa Bamrungsap, Ph.D.

National Nanotechnology Center, National Science and Technology Development Agency

Abstract

This project demonstrated the development of surface enhanced Raman scattering (SERS)-based biosensors for cancer screening which the systems combine high sensitivity of SERS technique together with magnetic enrichment for target analytes separation to improve specificity of the detection. Gold nanorods (AuNRs) which is one of the most effective SERS materials is selected to be a substrate due to its strong light absorption and scattering. Herein, a plasmonic paper was fabricated by simple immersing plain laboratory filter paper into AuNR solution and applied as a SERS substrate. The SERS property of the substrate was evaluated using 4-mercaptobenzoic acid (4-MBA), and rhodamine 6G (R6G), which showed the enhancement factor (EF) around 10⁶-10⁷. HT-29, a colorectal cancer cell line that highly expresses epithelial cell adhesion molecule (EpCAM) was used as a target cell, non-EpCAMexpressing cells, fibroblast and red blood cells (RBCs) were applied as negative controls. With the enhancement of AuNRs, intrinsic Raman signal of cells was then enhanced by SERS effect on the plasmonic paper. By using immunomagnetic specific to biomarkers expressed on cancer cells surface, we were able to collect the target cells from samples. The target was identified by observing intrinsic Raman signal of the cells which have distinctive fingerprint among normal and cancer cells or different cancer cells due to diverse expression of surface markers. To extend the application of SERS technique for biomolecule detection, we reported another detection system of microRNA-29a (miRNA-29a), which is a biomarker of cervical cancer. Here, a SERS tag was fabricated using AuNRs attaching with a Raman reporter molecule, 4-mercaptobenzoic acid (4-MBA), and a DNA probe specific to target miRNA. Magnetic nanoparticles conjugated with DNA probe complementary to the target was used to enrich target miRNAs from samples. The magnetic-RNAs complexes were then labeled with SERS tags to from sandwich complexes and the presence of the target miRNA was identified by signal of the SERS tag. The specificity of the system was evaluated using other miRNAs, miRNA-21 and miRNA-210. The success of this project has extended the feasibility of using SERS-based biosensors for the development of effective cancer screening methods.

Keywords Surface enhanced Raman scattering (SERS), gold nanorod, biosensor, cancer

บทคัดย่อ

โครงการนี้แสดงการพัฒนาใบโอเซ็นเซอร์ที่อาศัยหลักการของพื้นผิวขยายสัญญาณรามานสำหรับการตรวจคัดกรอง มะเร็ง ซึ่งระบบเซ็นเซอร์ดังกล่าวจะอาศัยความไวจากเทคนิคพื้นผิวขยายสัญญาณรามานและความจำเพาะจากการใช้อนภาค นาในแม่เหล็กในการแยกโมเลกุลเป้าหมายออกจากตัวอย่าง โดยอนุภาคทองนาโนแบบแท่งได้ถูกนำมาใช้เป็นวัสดุที่ทำหน้าที่ ขยายสัญญาณรามานเนื่องจากมีคุณสมบัติที่ดีในการดูดกลืนและกระเจิงแสง ในที่นี้กระดาษพลาสโมนิคสามารถเตรียมได้โดย การจุ่มกรองลงในสารละลายของอนุภาคทองนาโนแบบแท่งเพื่อนำมาใช้เป็นวัสดุรองรับและขยายสัญญาณรามาน โดย คณสมบัติการขยายสัญญาณรามานของกระดาษพลาสโมนิคที่เตรียมขึ้นสามารถทดสอบได้โดยใช้โมเลกลที่ให้สัญญาณรา มาน ได้แก่ 4-เมอร์แคปโตเบนโซอิกแอซิด และโรดามีน6จี ซึ่งพบว่ามีค่าการขยายสัญญาณอยู่ที่ 10⁶-10⁷ เท่า หลังจากนั้นได้ ้นำกระดาษพลาสโมนิคที่เตรียมขึ้นไปใช้ในการวัดสัญญาณรามานของเซลล์ โดยเลือก HT-29 ซึ่งเป็นเซลล์มะเร็งลำไส้ใหญ่ที่มี การแสดงออกของ epithelial cell adhesion molecule บนผิวเซลล์จำนวนมากเป็นเซลล์เป้าหมาย และใช้ไฟโบรบลาสต์ และ เซลล์เม็ดเลือดแดงเป็นตัวควบคุม ซึ่งพบว่าเซลล์ปกติและเซลล์มะเร็งจะให้รูปแบบสัญญาณรามานที่ต่างกันเนื่องจากมี องค์ประกอบและการแสดงออกของตัวบ่งชี้ที่ผิวเซลล์มีความแตกต่างกัน นอกจากนี้ได้ใช้อนุภาคอิมมูโนแม่เหล็กที่สามารถจับ จำเพาะและแยกเซลล์เป้าหมายออกจากตัวอย่างและสามารถระบการปรากภอย่ของเซลล์มะเร็งเป้าหมายได้จากสัญญาณรา มานที่วัดได้บนกระดาษพลาสโมนิค นอกจากนี้ได้ทำการพัฒนาระบบการตรวจวัดไมโครอาร์เอ็นเอเป้าหมายชนิด 29เอ ที่เป็น ตัวบ่งชี้ของมะเร็งปากมดลกด้วย SERS tag ซึ่งเตรียม SERS tag ได้โดยการติดโมเลกลรามานชนิด4-เมอร์แคปโตเบนโซอิก แอซิดและดีเอ็นเอโพรบที่จับจำเพาะกับไมโครอาร์เอ็นเอเป้าหมายได้บนอนภาคทองนาโนชนิดแท่ง ซึ่งการตรวจวัดทำได้โดยใช้ อนุภาคนาโนแม่เหล็กติดฉลากดีเอ็นเอโพรบที่จับกับไมโครอาร์เอ็นเอเป้าหมายด้านหนึ่งเพื่อจับและแยกไมโครอาร์เอ็นเอ เป้าหมายออกจากตัวอย่างจากนั้นเติม SERS tag เพื่อจับกับไมโครอาร์เอ็นเอเป้าหมายอีกด้านหนึ่ง ดังนั้นจะสามารถระบุการ ปรากภูของไมโครอาร์เอ็นเอเป้าหมายในตัวอย่างได้โดยการตรวจวัดสัญญาณของ SERS tag นอกจากนี้ได้ทำการทดสอบ ความจำเพาะของระบบด้วยไมโครอาร์เอ็นเอชนิดอื่นๆ ได้แก่ ไมโครอาร์เอ็นเอ-21 และไมโครอาร์เอ็นเอ-210 ซึ่งพบว่า SERS tag ที่พัฒนาขึ้นนี้มีความจำเพาะกับไมโครอาร์เอ็นเอเป้าหมายและไม่จับกับไมโครอาร์เอ็นเอชนิดอื่นๆ ซึ่งผลจากการศึกษาจาก โครงการนี้สามารถแสดงให้เห็นความเป็นไปได้ในการพัฒนาไบโอเซ็นเซอร์ที่อาศัยหลักการขยายสัญญาณรามานสำหรับการ ตรวจคัดกรองมะเร็งได้

คำสำคัญ พื้นผิวขยายสัญญาณการกระเจิงแสงรามาน, อนุภาคทองนาโนแบบแท่ง, ไบโอเซ็นเซอร์, มะเร็ง

Introduction

Cancer is currently one of the most lethal diseases concerns in worldwide. The early and precise cancer diagnostic can increase the chances for successful treatment and improve survival rates of cancer patients. With this fact, the demand for specific and accurate cancer screening has driven the development of novel diagnostic tools having high sensitivity and specificity. Due to the advance in nanotechnology, nanomaterial-based platforms together with several optical measurement techniques including fluorescence, surface plasmon resonance (SPR), and colorimetry, have been employed for cancer cells and biomarkers detection. Surface enhanced Raman scattering (SERS) has become an important tool for specific biomolecules detection in recent years due to advantages in high sensitivity at single molecule level. The unique "fingerprint" Raman spectra of particular molecules can provide the identification and quantitation of specific targets. Moreover, high spatial resolution and utilization of a single wavelength excitation allow multiplex detection. In SERS, the enhancement can be achieved when Raman molecules are in close proximity to metallic surface on the 10 to 100 nm scale [1]. The chemical composition, size, and shape of the metal substrate can greatly affect the electromagnetic field enhancement. Besides spherical shape, anisotropic geometries like triangles, cubes, stars, and rods, provide advantages in producing concentrated field called "hot spots" at the tips; therefore, strong SERS signal can be generated [2]. Gold Nanorod (AuNR) is one of materials that have been extensively used as SERS active substrates. Due to their anisotropic geometries, AuNRs exhibit two plasmon bands: transverse band at the lower wavelength, and tunable longitudinal band at near-infrared region. AuNRs are chemically stable, and their size including shape are easily to be controlled during the synthesis [3]. Moreover, strong thiol-gold interaction facilitates conjugation of Raman reporters and targeting ligands for specific target recognition which make AuNRs suitable for the fabrication of SERS biosensors.

Nowadays, Raman measurement can be conveniently operated in laboratory and industrial scenarios using a benchtop Raman spectrometer. Furthermore, the analytes detection at a field test can be easily performed by a handheld Raman spectrometer in solution or on a solid substrates with high efficiency. Therefore, the application of SERS biosensors for point-of-care diagnostic is also possible. Generally, there are two main principles of SERS-based detection including intrinsic and extrinsic detections [4]. For the intrinsic approach, target analytes will be absorbed or located on a "SERS substrate" which is a rough metallic surface or arrays of metallic nanoparticles on a solid support. The intrinsic Raman signal of the analytes is directly detected by the help of electromagnetic field enhancement of a SERS substrate. Targeting ligands such as antibody, peptide, aptamers, or small molecules can also be immobilized onto a SERS substrate to capture target molecules. In this case, Raman spectral differences between before and after target capture can be used to identify the species. The intrinsic approach provide advantages in simplicity and short-time analysis because it is a label free technique and no need

to wash labeling molecules. For the intrinsic SERS-based biosensor, SERS substrate is a key factor to achieve highly effective detection of target molecules. Numbers of SERS substrates varied from roughened noble metal surfaces to patterned metal nanostructures with enhancement factors ranging from 10⁴ to 10¹⁰ have been demonstrated over the last two decades [5]. Several techniques which are top-down and bottom-up approaches have been used to fabricate SERS substrates such as e-beam lithography, colloidal lithography, on-wire lithography, and self- and directed-assembly, which enable precise control over the size, shape, and organization of the metal nanostructures [6]. However, preparation of rigid SERS substrates using those techniques are time consuming, high cost of production, and require sophisticated equipment. Therefore, the development of cost-effective and scalable SERS substrates is highly desirable. Recently, soft material like paper has been coated with metallic nanoparticles, defined as a plasmonic paper, and reported as an effective SERS substrate. Paper-based substrates provide advantages in cost effective, mechanically favorable (easy to be cut or shape), and easily disposable. The porous structure of paper also provides large surface area suitable for high amount of nanoparticle absorption compared to flat surfaces. Moreover, the paper can act as a microfluidic for liquid sample transportation and the analytes can be concentrated at specific area by solvent evaporation.

For the extrinsic detection, targets will be labeled with "SERS tag" which provide strong and unique fingerprint and the presence of targets can be identified by Raman signal of the SERS tags. Typically, SERS tags consist of four counterparts: metal nanoparticles, Raman molecules, protecting layers, and targeting ligand. To realize strong SERS effect, it is necessary to design metallic core or substrate that can lead to maximum optical field, resulting in maximum Raman signal enhancement. Raman reporter molecules will be attached to metal core to generate strong and specific fingerprints. Protecting layer such as bovine serum albumin (BSA), polyethylene glycol (PEG), and silica, is added to cover the metal core to prevent dissociation of reporters and enhance stability and biocompatibility of the SERS tags [7]. Targeting ligands such as antibody, aptamer, oligonucleotide probe, or small molecules are cross-linked to the SERS tags to provide specificity to biological targets. The extrinsic approach provides advantages in high sensitivity, multiplexing capability, and ability to be used in complex systems. Besides protein, pathogen, and cell detection, DNA and RNA identification via extrinsic SERS has been reported extensively. Generally, SERS tags will be conjugated to DNA probes specific to target oligonucleotides. Upon hybridization, target DNA or RNA will bind with the complementary probes attached on SERS tags and the presence of the target oligonucleotides will be identified by Raman signal of the SERS tags. Using multiple SERS tags can also facilitate multiplex detection of DNAs and RNAs that are associated with diseases. Due to many advantages of extrinsic SERS and strong DNA:RNA base-pair interaction, multiplex detection of miRNAs which are biomarkers of cancers is feasible.

MicroRNA (miRNA) is a group of single-stranded, small (18-25 nucleotide), noncoding RNAs that regulate the expression of target genes. It has been reported that alteration of miRNA expression is related to the initiation

and progression of several human cancers [8]. Based on profiling of hundreds of normal tissue and cancers, it is found that tumorigenesis and progression are relevant with not a single type of miRNA but with many miRNAs. For example, several miRNAs such as miRNA-21, miRNA-215, miRNA-140, and miRNA-502 are found to be associated with colon cancer [9]. MiRNA-34, miRNA-200, miRNA-205, and let-7 have played a role in breast cancer pathogenesis through the loss of their tumor suppressor properties [10]. Therefore, detection of miRNAs will be useful for diagnosis and prognosis of cancer as well as determination of treatment response. Conventional miRNAs identification are commonly based on 3 methods including Northern blotting analysis, miRNA microarray, and quantitative RT-PCR (qRT-PCR) [8]. Each methodology has its own strength and weakness. For example, Northern blotting requires larger amount of total RNA, and often fail to detect low abundance of miRNA. Microarrays are less expensive, however provide low sensitivity and narrow dynamic range of detection. qRT-PCR has high accuracy and dynamic range but suffer from throughput tissues. Therefore, it is still necessary to develop a new platform that provide high sensitivity and multiplexing ability with wide dynamic range for accurate detection of low abundance miRNAs in samples.

In this project, we demonstrated two different systems of SERS-based detection for cancer screening. In the first system, we focused on the intrinsic target cells detection using a paper-based SERS substrate. The target cells were enriched by immunomagnetic conjugates specific to biomarkers expressed on the cells surface prior to SERS detection. A SERS substrate was prepared conveniently by coating a piece of filter paper with AuNRs solution. The intrinsic Raman signal of the captured cells were measured with the help of the field enhancement by a paper-based SERS substrate. With the high sensitivity of SERS-based technique and background interference reduction by immunomagnetic separation, the paper-based SERS combining with magnetic isolation could provide advantages as a cost effective, rapid, and sensitive detection method. The second platform focused on the detection of miRNA-29a which is cancer biomarker using SERS tags. Magnetic nanoparticle conjugated with DNA probe complementary to the target miRNA was also applied to capture the target miRNA from samples. The magnetic-RNAs complexes were then labeled with SERS tags to from sandwich complexes and the presence of the target miRNA was identified by signal of the SERS tags.

Objectives

- 1. To synthesize AuNRs with controlled size and aspect ratio as SERS substrates
- 2. To prepare a paper-based SERS substrate for target cells detection by enhancing intrinsic Raman signal of main components on cells surface such as protein, lipid, or DNA which are different among cancer and normal cells
- 3. To fabricate SERS tags providing strong Raman signal and high stability by attaching Raman reporter molecules and DNA probes onto AuNRs surface for target miRNA labeling

- 4. To develop and apply magnetic conjugates for specific target enrichment in order to isolate and purify the target cells and miRNAs from samples which will reflect in better specificity and sensitivity of the detection
- 5. To establish a paper-based SERS platform which is simple and cost-effective for target cancer cells detection
- 6. To demonstrate miRNA detection which is a biomarker of cancer using SERS tags which will benefit cancer screening at the early stage

Methodology

The methodology of this project is divided into two main parts as followed:

1. Paper-based SERS substrate for cancer cell detection

1.1 AuNRs synthesis

AuNRs were synthesized based on a modified seed mediated growth method by using a surfactant, hexadecyltrimethylammonium (CTAB), as a template and NaBH₄ as a reducing agent as described in the previous work [11]. The CTAB acts as a building block to control size, shape, and aspect ratio of the AuNRs which affects their absorption and scattering reflecting in the enhancement of Raman signal. The UV-VIS spectrometer were used to verify absorption spectrum of AuNR solution. The size and shape of synthesized AuNRs were characterized using TEM analysis. The as-prepared AuNRs were then further used for SERS substrate preparation.

1.2. Preparation of plasmonic paper

The plasmonic paper was prepared by coating AuNRs on laboratory filter paper. The filter paper was cut to 1 x 1 cm² and immersed into petri dish containing AuNR solution at room temperature overnight. The plasmonic paper was rinsed with deionized water and dried for 30 minutes. The distribution of AuNRs on the paper substrate was examined through scanning electron microscope (SEM) using FE-SEM SU8030, Hitachi, japan. To evaluate the Raman enhancement property, the plasmonic paper was dipped in different concentrations of 4-mercaptobenzoic acid (4-MBA) and rhodamine6G (R6G) solution separately for 30 minutes and dried. SERS measurement was performed using a Raman spectrometer (NT-MDT, Russia) coupled with an inverted confocal microscope (Olympus IX7, Olympus, USA). A He-Ne laser at wavelength of 633 nm through 100X objective lens was utilized to excite samples. SERS spectra from 5 different locations were collected for each concentration of 4-MBA and the SERS intensities were averaged for enhancement factor calculation.

1.3 Immunomagnetic conjugates preparation and target cell enrichment

To prepare immunomagnetic conjugate, 0.1 mg of 1 μ m carboxylated magnetic particles was suspended in MES buffer (pH 5.5). Then 0.1 mg 1-ethyl-3-(3-dimethylaminopropyl)carbodiimide hydrochloride (EDC) and 0.2 mg N-hydroxysuccinimide (NHS) were added to activate carboxyl groups on the magnetic beads to form active esters. The activated magnetic beads were then exchanged into phosphate buffer saline (PBS) pH 7.4 and incubated with 5 μ g EpCAM-specific antibody for 3 h on ice. Excess antibodies and reagents were removed by

magnetic separation using a magnet attaching to the side of Eppendorf tubes followed by removal of supernatant liquid. Then the immunomagnetic conjugate was washed twice and kept in PBS containing 0.1 % Tween-20 and 0.1 % of bovine serum albumin (BSA) at 4°C. A colon cancer cell line, HT-29, with highly expressed EpCAM (epithelial cell adhesion molecules) biomarker was selected as a target cell while the non-EpCAM expressed cells including, fibroblast and red blood cells (RBCs) were used as negative controls. HT-29 cell line was cultured with McCoy's 5A medium supplemented with 10% fetal bovine serum, penicillin (10000 units/mL), and streptomycin (10 mg/mL). Fibroblast that does not express EpCAM was cultured in DMEM supplemented with 10% fetal bovine serum, penicillin (10000 units/mL), and streptomycin (10000 μg/mL). Both cell lines were cultured in humidified atmosphere at 37 °C with 5 % CO₂. Before performing experiments, cells were harvested by trypsinization, washed and re-suspended in 10 mM phosphate buffered saline (PBS). The number of cells was counted using a hemocytometer through an inverted microscope (Olympus CKX41, USA). The 10 μg/mL of immunomagnetic conjugates were incubated with the samples containing target cells, non-target cells, or cell mixture on ice. After 30 min of incubation, magnetic field was applied to collect the target cells for further detection.

1.4 Detection of target cell on a plasmonic paper

Prior to perform target cell detection, we first collected SERS spectra of target cells and non-target cells on plasmonic papers as a library. The target cells separated by immunomagnetic were dropped on a plasmonic paper and the spectra of the cells were collected at several different positions. SERS spectra of cells deposited on the plasmonic paper were obtained using a Raman spectrometer (NT-MDT, Russia) coupled with an inverted confocal microscope with the laser power of 0.17 mW and exposure time of 20 s with 3 accumulations. The SERS spectra of 20 samples (n = 20) from each cell type with different locations from each sample were collected in the range of 100–1900 cm⁻¹ and baseline subtraction was performed by the software package WIRE 4.2 (Renishaw). The presence of target cells was identified by comparing SERS spectra of the captured cells with the library spectra which was differentiated by distinctive patterns among the target cells and non-target cells. A combination of principal component analysis (PCA) and k-nearest-neighbor algorithm (k-NN) was performed on 20 different data sets for each cell type including the enriched cells for comparison and identification using scikit-learn software.

2. Detection of miRNA which is a biomarker of cervical cancer using SERs tag

2.1 SERS tags fabrication

The SERS tag was prepared by attaching Raman reporters, 4-MBA, on AuNRs surface. Briefly, AuNR solution was gently mixed with 20 mM 4-MBA for 3 h at room temperature. The coated AuNRs were then separated from the solution, washed by centrifugation, and then stored at room temperature. The solutions of 4-MBA coated AuNRs were mixed with 2 mM mPEG-SH solution and 10 μ M thiolated DNA probe, P1, complementary to the target miRNA-29a for 12 h incubation at room temperature. The sequences of DNA probes, target, and non-target miRNA

were listed in Table 1 as followed. Raman spectra of SERS tags were measured to confirm that they can be used to generate signal for further target detection.

Table 1: list of oligonucleotides

Name	Sequence
P1	5' - SH- TTT TTT TTA ACC GAT TTC - 3'
P2	5' - AGA TGG TGC TAT TTT TTT - NH ₂ - 3'
miRNA-29a	5' - uag cac cau cug aaa ucg guu a - 3'
miRNA-21	5' - uag cuu auc aga cug aug uug a - 3'
miRNA-210	5' - cug ugc gug uga cag cgg cug a - 3'

2.2. Magnetic conjugates preparation and target miRNAs enrichment

Magnetic conjugates were prepared for targets miRNA separation and enrichment from samples prior to the detection. The carbodiimide chemistry were used to conjugate MNP containing carboxyl groups with amine groups of DNA probe, P2, specific to target miRNA-29a similar to the preparation of immunomagnetic conjugates as mentioned above. Briefly, 0.5 mg of 200 nm MNPs were treated by 0.5 mg EDC and 0.5 mg NHS to activate carboxyl groups of the particles. After activation, 15 μ L of 10 μ M DNA probe, P2 was added and incubated overnight. The MNP-DNA probes were washed twice by centrifugation and resuspend in PBS at the concentration 1 mg/mL. The miRNA-29a over expressed in cervical cancer with various concentration was selected as a target. The DNA probe-magnetic conjugates at the final concentration at 10 μ g/mL was incubated with the samples containing the target miRNAs or control on ice for 30 min. After the incubation, a magnetic bar was used to collect the target miRNAs for SERS measurement. The specificity of the system was also performed using non target miRNA including miRNA-21 and miRNA-210.

2.3 miRNA detection by SERS tags

The SERS tags 10 μ L was added into the captured miRNA solution and incubated on ice for 30 min to form sandwich complexes. After incubation, a magnet bar were used to collect the complexes and SERS spectra of miRNAs labeled with SERS tags were measured using a benchtop Raman spectrometer with the laser output power at 400 mW, accumulation time 10 s, and N = 10. In this case, we verified the presence of miRNAs by Raman signal of SERS tags that specifically bind to each type of target miRNAs.

Results and Discussion

1. Paper-based SERS substrate for cancer cell detection

Here, we demonstrated a system of plasmonic paper as a SERS substrate combined with magnetic separation for cancer cell screening as depicted in Figure 1.

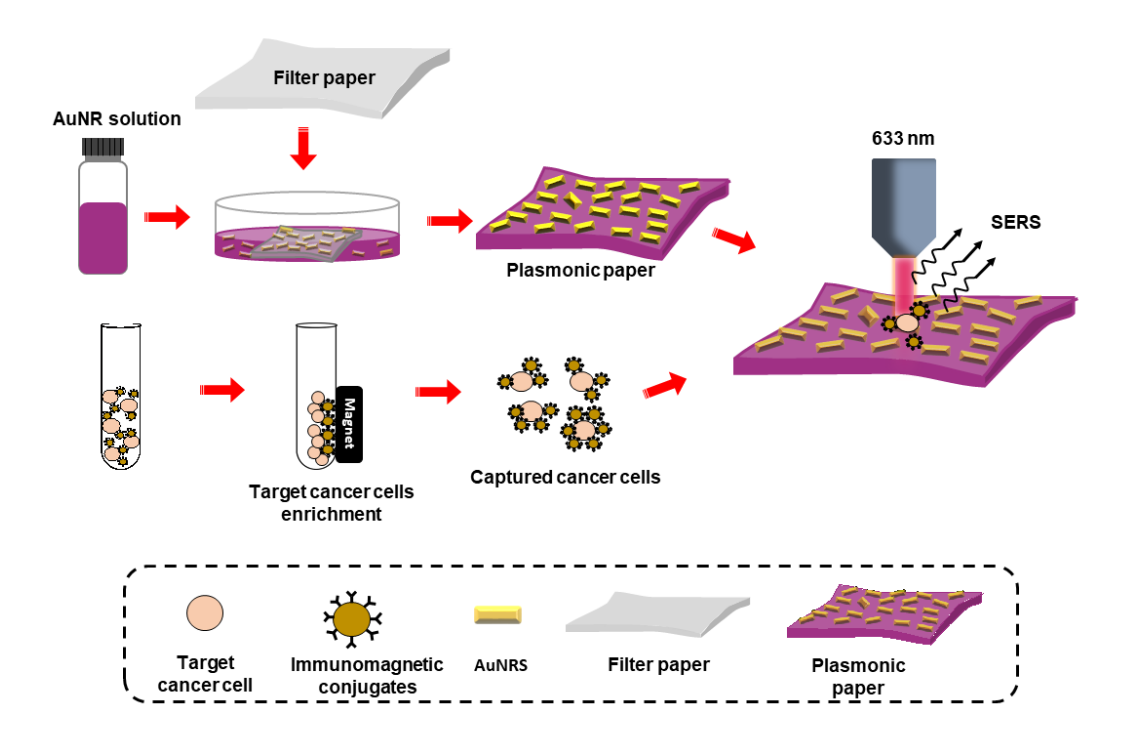


Figure 1. Schematic diagram illustrating the plasmonic paper fabrication and cancer cell detection with the assistance of magnetic enrichment.

1.1 Plasmonic paper fabrication and characterization

The plasmonic paper was fabricated starting with AuNR synthesis by seed mediated growth method using CTAB as a surfactant. As shown in Figure 2A, the AuNRs presented transverse and longitudinal absorption bands at 526 and 696 nm, respectively, according to the oscillation of electrons along their facets. The TEM image inset reveals the average width and length of 16 ± 2 nm and 51 ± 5 nm with the aspect ratio (length divided by width) of 3.2. To prepare plasmonic paper, laboratory filter paper with the size of 1 × 1 cm² was immersed into AuNR solution overnight twice. After immersing, a dark red-purple color was observed from the paper indicating successful loading of the AuNRs on the paper. Surface plasmon resonance (SPR) absorption of the plasmonic paper was observed with blue shift and broader bands compared with that of the AuNR solution as shown in Figure 2A. This change is due to the alteration of dielectric ambient after loading AuNRs on the paper resulting in the decrease of refractive index [12]. Figure 2B shows the surface morphology of plain laboratory filter paper including different layers of fiber by SEM image. After coating, AuNRs were distributed throughout the fiber without aggregation as demonstrated in SEM images (Figure 2C and 2D). AuNRs were deposited firmly on three dimensional structure of the paper due to electrostatic interaction between the positive charge of CTAB capping AuNRs and the negative charge of the hydroxyl-rich cellulose paper [13]. It was observed that high amount of AuNRs assembled on the

paper surface with an approximate number of $188 \pm 20 \text{ NPs/}\mu\text{m}^2$. With high density of AuNRs, intensive electromagnetic field can be produced from several hotspots generated by AuNRs located on the plasmonic paper surface with suitable inter-particle distance [14]. This effect intensifies the local light absorption and scattering, resulting in high signal enhancement ability of the plasmonic paper [15-17].

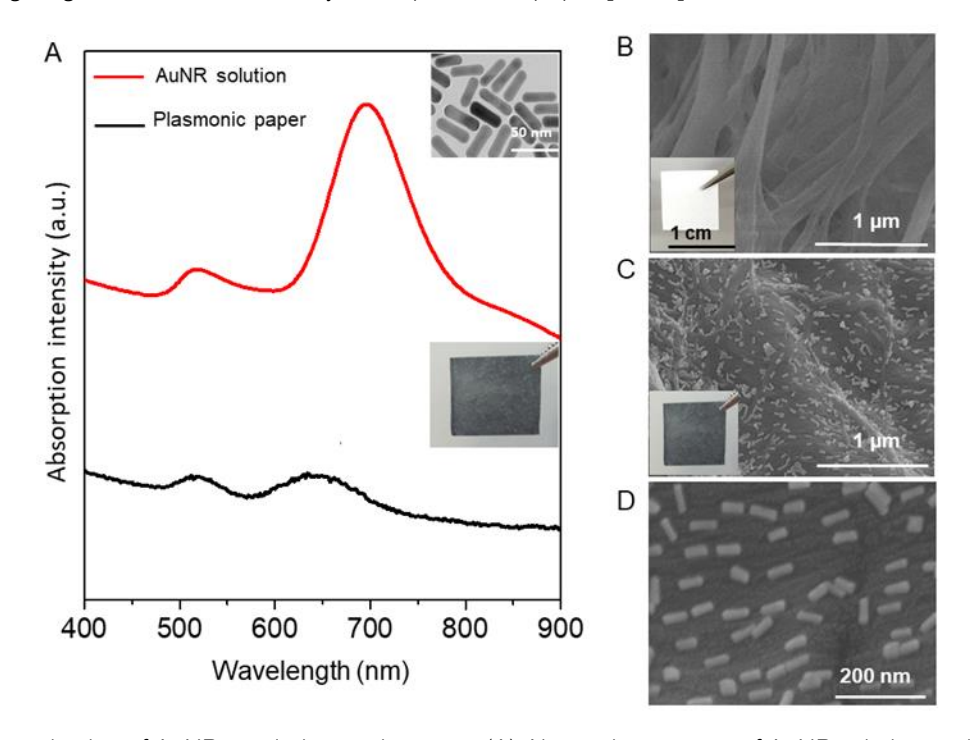


Fig. 2. Characterization of AuNRs and plasmonic paper. (A) Absorption spectra of AuNR solution and the plasmonic paper. (B) SEM image of bare filter paper. (C-D) SEM images of the plasmonic paper (AuNR coated).

To evaluate the enhancement property of the plasmonic paper, a typical Raman active molecule, 4-MBA, was loaded on the paper. The plasmonic paper and filter paper were dipped in different concentrations of 4-MBA solution ranging from 0.1 nM to 1 M for 30 min. SERS and Raman spectra of 4-MBA were then obtained from five different random locations on each substrate. The most intense characteristic Raman shift of 4-MBA appearing on the paper at 1590 cm⁻¹ was assigned to ring breathing mode of (C-C) [18] and was selected and averaged for EF calculation using following equation, the derivation of which is demonstrated in supplementary material [19]:

$$EF = \frac{I_{SERS}}{I_{Raman}} \times \frac{C_{Raman}}{C_{SERS}} \tag{1}$$

where I_{SERS} is the SERS intensity of 4-MBA on the plasmonic paper, C_{SERS} is the concentration of 4-MBA on the plasmonic paper, I_{Raman} is the Raman intensity of 4-MBA on a filter paper, and C_{Raman} is the concentration of 4-MBA on a filter paper. Based on SERS intensity at 1590 cm⁻¹, the EF of the plasmonic paper was calculated to be about

10⁷ -10⁸ (**Table 2**) with the detection limit of 1 nM (**Figure 3**), which is consistent with other paper-based SERS substrates that were previously reported by other research groups [20,21]. To eliminate the selective enrichment of the analytes on the plasmonic paper due to strong thiol-gold affinity between 4-MBA and AuNRs, rhodamine 6G (R6G), which does not have such interaction with the substrate, was also applied. Utilization of R6G resulted in an EF in the similar range of 10⁶ -10⁷, as demonstrated in **Figure 4** and **Figure 5**, and **Table 3**. The fabrication of SERS substrate using this technique is not only simple and cost-effective, but the resulting plasmonic paper also shows good enhancement property and feasibility for target analyte detection.

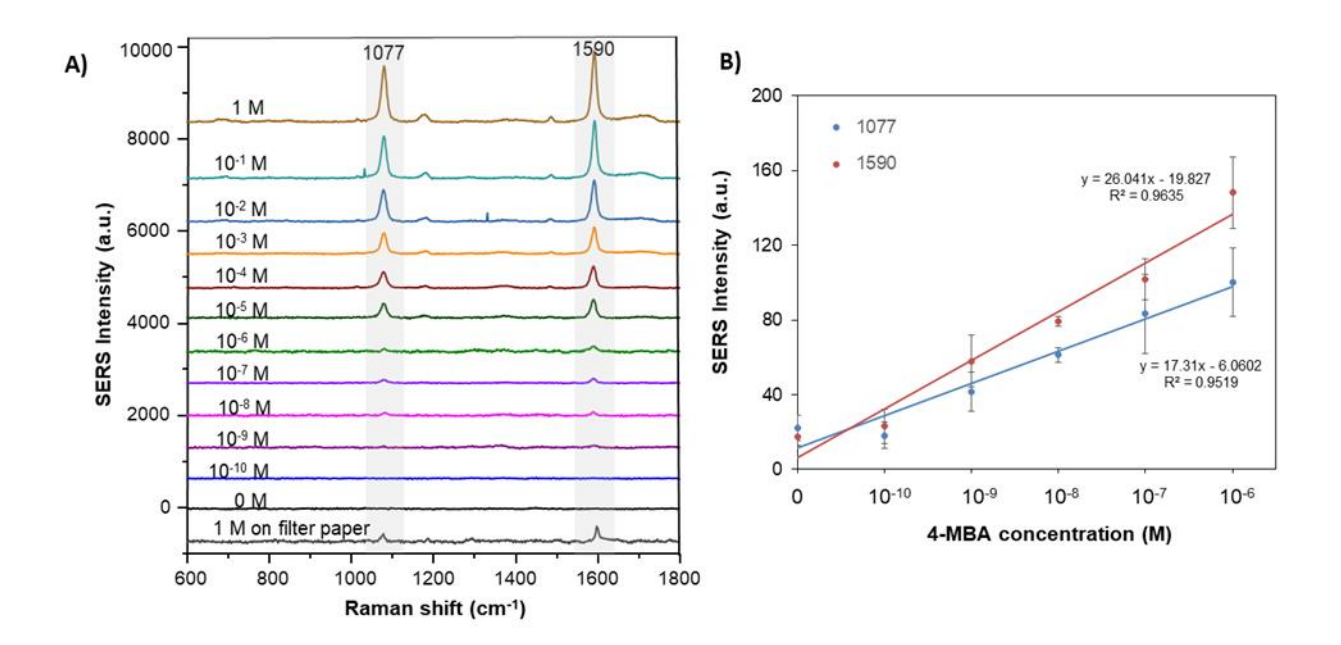


Figure 3. Raman enhancement property of the plasmonic paper. (A) SERS spectra at different concentrations of 4-MBA obtained on the plasmonic paper. (B) Plot demonstrating the relationship of 4-MBA concentrations and SERS intensities at 1077 and 1590 cm⁻¹ on the plasmonic paper.

Table 2. Enhancement factor of plasmonic paper by 4-mercaptobenzoic acid (4-MBA) compared with filter paper calculated using Raman shift at 1590 cm⁻¹

C _{Raman}	 Raman	C _{SERS}	I _{SERS}	I _{SERS} / I _{Raman}	C_{Raman}/C_{SERS}	EF
(101)					7	
1	102	100	86	0.83675212	10'	8.4×10^6
1	102	10	67	0.65240067	10 ⁸	6.5×10^{7}
1	102	1	42	0.40942527	10 ⁹	4.1×10^{8}

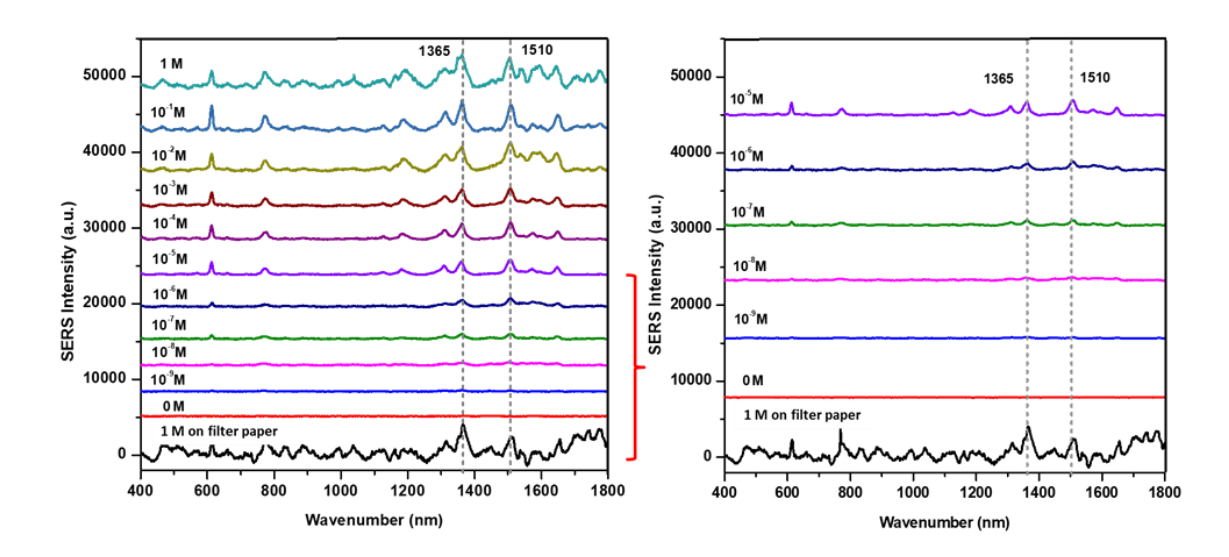


Figure 4. R6G structure and SERS spectra of R6G at different concentrations obtained on the plasmonic paper

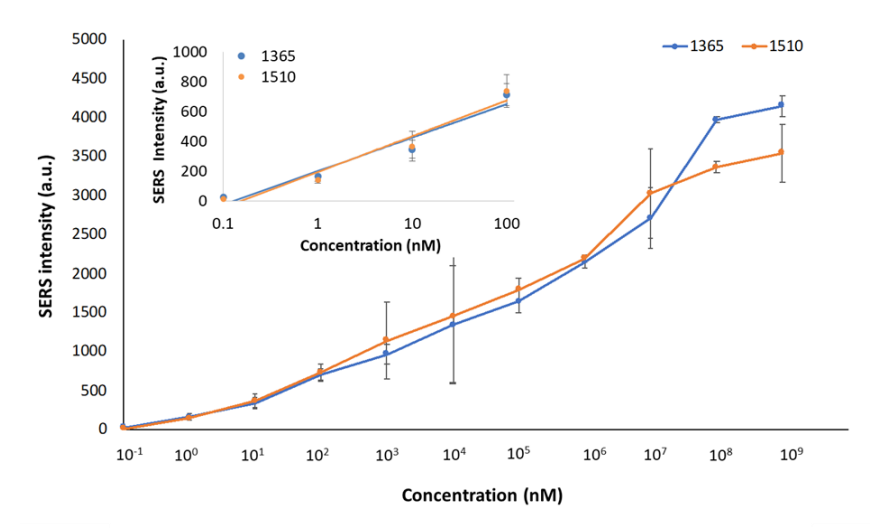


Figure 5. Plot of SERS intensities at 1365 and 1510 cm⁻¹ corresponding to concentrations of R6G on the plasmonic paper.

Table 3. Enhancement factor of plasmonic paper by Rhodamine 6G (R6G) compared with filter paper calculated using Raman shift at 1510 cm⁻¹

C _{Raman}	Raman	C _{SERS}	I _{SERS}	SERS Raman	C_{Raman}/C_{SERS}	EF
(M)		(nM)				
1	2147	100	738	0.343735	10 ⁷	3.4×10^{6}
1	2147	10	366	0.016768	10 ⁸	1.7×10^{6}
1	2147	1	142	0.066139	10 ⁹	6.6×10^{7}

3.2 SERS spectra of cancerous cells, fibroblast, and RBCs

Prior to performing the detection and identification of the target cancer cells from samples, SERS spectra of cancerous cells (HT-29), normal cells (fibroblast), and RBCs were acquired on the plasmonic papers. The cell suspension containing each cell type was dropped and dried on the plasmonic paper. After drying, the cells were dehydrated resulting in membrane damage and cytoskeletal changes. Therefore, we presumed that not the whole cells but fractions of cells likely contacted with the plasmonic paper after cell death. Moreover, some intracellular components such as DNA fragments from nuclear matrix could have leaked and interacted with the plasmonic paper. As a result, SERS spectra achieved on the plasmonic paper would contain information of biomolecules from both cell surface and intracellular components. As demonstrated in Figure 6, all cells yielded strong SERS signal demonstrating excellent enhancement performance of the plasmonic paper, with different fingerprints among various cell types corresponding to results achieved in another study [22]. Metabolically active cancer cells are known to produce large amount of protein and nucleic acid, resulting in dominating signature bands of protein components and nucleic acids. Here, the average SERS spectrum of HT-29 cells showed intense bands of protein at 758-760 cm⁻¹ (ring breathing), 1175-1177 cm⁻¹ (C-H), 1207-1209 cm⁻¹ (C-C), 1550-1555 cm⁻¹ (N-H), and 1615-1620 cm⁻¹ (C=C) as listed in Table 4 due to high amounts of antigens and receptor proteins presented on cancerous cell surface [12, 24-26]. Nucleic acid-dominated spectra were observed by relatively strong bands of ring breathing at 680 cm⁻¹, 916 cm⁻¹, 1479-1491 cm⁻¹, and 1572-1578 cm⁻¹ because of large nuclei feature of cancer cells [23-25]. In addition, the bands at 1265 cm⁻¹ (C-H) and 1655-1680 cm⁻¹ (C=C) from phospholipid were comparatively weak because of loss in the architectural arrangement of lipid layers in cancerous cells. In contrast, healthy cells possess phospholipid-rich structure and lipid-layers in cell membrane. Therefore, the fibroblast cells (Figure 6) showed dominant lipid-spectra at 1265 cm⁻¹ (C-C), 1350 cm-1 (CH/CH₂), and 1655-1680 cm⁻¹ (C=C), as described earlier [24,26]. In addition, SERS spectrum of RBCs was investigated and specific bands were assigned as shown in Figure 6. The spectrum was rich at wave number 754 cm⁻¹ (ring breathing), 1367 cm⁻¹ (ring stretching), and 1582-1586 cm⁻¹ (C-C), representing vibration modes of porphyrin, which is a main component of heme groups of hemoglobin [27-30]. It was reported that 33% of RBCs consists of hemoglobin; thus, the porphyrin-dominated spectra were observed [29]. Furthermore, other non-porphyrin bands related to components of hemoglobin protein vibrational modes were evident, such as 1175-1177 cm⁻¹ (C-H), 1440 cm⁻¹ (CH_a), 1550-1555 cm⁻¹ (N-H), and 1615-1620 cm⁻¹ (C=C), respectively. The different fingerprints between cancerous cells, fibroblasts, and RBCs make the plasmonic paper promising for cancer screening.

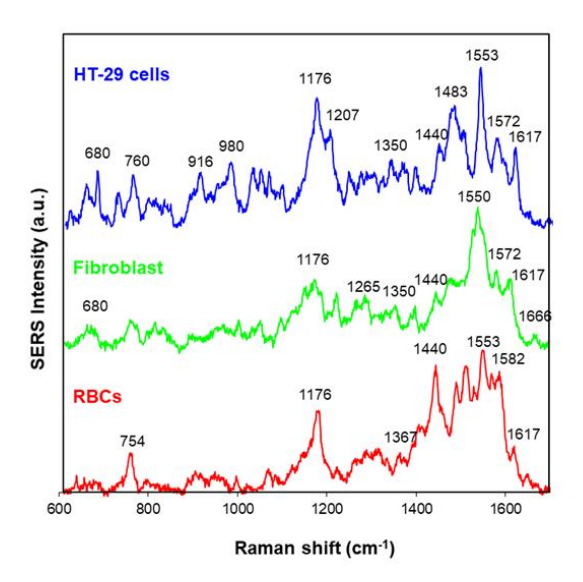


Figure 6. SERS spectra of cancerous cells (HT-29) and non-cancerous cells (fibroblast and RBCs) on the plasmonic paper.

Table 4 Raman peak positions and tentative vibrational mode assignment observed in this study.

Peak position ^a	Vibrational mode	Tentative assignment	References
680	Ring breathing	DNA/RNA (guanine)	24
754	Ring breathing	porphyrin	27-29
758-760	Ring breathing	Tryptophan	23, 25
916	Ring breathing	DNA/RNA(furanose)	25
980	C-C stretching	$oldsymbol{eta}$ sheet	23
1175-1177	C-H bending	Tyrosine	23, 25
1207-1209	C-C stretching	Phenylalanine, Tryptophan, Tyrosine	23, 25
1265	C-H deformation	lipid	24
1350	CH ₃ /CH ₂ twisting	lipid	24
1367	Half-ring stretching	porphyrin	28
1437-1440	CH ₂ deformation	lipid, protein	22, 23, 25
1479-1491	Ring breathing	DNA/RNA (adenine, guanine)	25
1550-1555	N-H	Tryptophan	22, 25
1572-1578	Ring breathing (C-C)	DNA/RNA (adenine, guanine)	23, 25
1582-1586	C-C asymmetric stretching	hemoglobin	27-29, 30
1615-1620	C=C	Tryptophan, Tyrosine	23, 25
1655-1680	C=C	lipid	26

^a approximate wavenumber range obtained in this study associating with the references

3.3 Detection of target cancer cells in mixture samples

Biological and clinical samples containing not only the target cancer cells but also normal cells, blood, and other biomolecules yielded complex SERS spectra resulting in complication of target cell analysis. Consequently, separation and enrichment processes are desirable to increase purity of the target and concentrate the limited amount of analytes in real samples. Magnetic separation and enrichment technique, with the advantages of ease of usage, low cost, and short processing time, have been intensively applied to capture target biomolecules to improve efficiency of detection [31]. In this study, immunomagnetic conjugates were prepared by functionalization of magnetic particles with EpCAM-specific antibody in order to recognize EpCAM-overexpressing colon cancer cells, HT-29. The conjugation was performed by carbodiimide chemistry through activation of carboxyl groups coated on magnetic beads in order to couple with amine groups of antibody. The successful conjugation was confirmed through the reduction of total negative charge of magnetic beads from -22.7 to -10.97 mV influenced by positive charge of amine groups on antibody. Prior to performing target cell enrichment in complex samples, capture efficiency of immunomagnetic conjugates was determined. The immunomagnetic conjugate was applied to capture and separate the target from a sample containing 5000 HT-29 cells spiked in PBS. After counting the enriched cells under a microscope, it was observed that the target cells were captured with high percentage above 80% demonstrating good capture efficiency. To evaluate non-specific interaction of immunomagnetic conjugates, similar amounts of non-target fibroblast cells were spiked in PBS and enriched with a similar procedure independently. The result showed that less than 25% of non-target cells were captured by immunomagnetic conjugate. This result revealed that the immunomagnetic conjugate provided good affinity towards the target cells via strong and specific recognition between antibodies on the surface of the particles and EpCAM overexpressed on the target cell. Additionally, the specific binding between immunomagnetic conjugates and target cells was much stronger than non-specific interaction due to interferences.

In order to demonstrate the detection of the target cells in biological samples that normally contain both cancer and normal cells, the target HT-29 cells were mixed with different amounts of non-target fibroblasts [HT-29:fibroblast in PBS, 5000:5000 (1:1), 5000:10000 (1:2) and 5000:25,000 (1:5)] followed by addition of 10 μ g/mL of immunomagnetic conjugates. The results showed that the cells were captured with high percentage of 84.16 %, 83.20 %, and 85.68%, from the mixed samples of 1:1, 1:2, and 1:5 ratios, respectively (Table 5).

Table 5. Percentage of the captured cells using immunomagnetic conjugate from mixed HT-29 cells and fibroblast samples (n = 6)

Number of cells	Number of captured cells	% capture
(HT-29:fibroblast)		
5,000:5,000	4,208	84.16
5,000:10,000	4,160	83.20
5,000:25,000	4,284	85.68

After target cell separation by immunomagnetic conjugates, the enriched samples from the 1:1 HT-29:fibroblast mixtures were verified through SERS spectra by dropping them on the plasmonic paper offering labelfree and non-invasive detection. The average spectra of captured cells showed intense bands at 1176 cm⁻¹ (C-H), 1553 cm⁻¹ (N-H) due to large amount of protein, and strong DNA band at 1572 cm⁻¹ (C-C) corresponding to the fingerprint of HT-29 cells as demonstrated in Figure 7A. However, shifted bands and slightly different fingerprint of the captured cells compared with that of the single HT-29 cell type were observed. The spectral deviation might derive from the captured cell suspension containing immunomagnetic conjugates (the spectrum is shown in Figure 8) and some of fibroblast cells that were contaminated through non-specific interaction. It is not always reliable to analyze SERS spectra of complicated and heterogeneous sample by naked eyes; hence, a combination of two multivariate data analysis techniques, namely principal component analysis (PCA) and the k-nearest-neighbor algorithm (k-NN), was applied. PCA is widely used in spectral analysis to reduce dimension of the original data set to a few principal components (PCs) with maximized variance within a group of data. In particular, dominant spectral peaks shown in HT-29 and fibroblast including 760, 980, 1176, 1207, 1350, 1440, 1483, 1553, 1572, and 1617 cm⁻¹ ¹ as labeled in **Figure 7A** were selected for analysis and PCA was used to reduce the dimension of the acquired Raman spectra to one. Figure 7B illustrates the PCA plot from 20 samples of each group showing the relationship between spectra of single HT-29 cells (blue), single fibroblasts (green), and the captured cells (black). It can be seen that the plot of each group was clustered indicating similarity and reproducibility of SERS spectra. The resulting 1-dimensional data were then classified as either HT-29 cells or fibroblasts using the k-NN algorithm with a sensitivity of 84.8% and specificity of 82.6%, representing diverse fingerprints among cancerous and non-cancerous cells. To analyze and classify the captured cells, the spectra acquired from both the HT-29 and fibroblast were again used to construct both PCA and k-NN classifier. Then, the constructed classifier was applied to identify the captured cells as cancerous cells (HT-29) resulting in an accuracy of 83.7%.

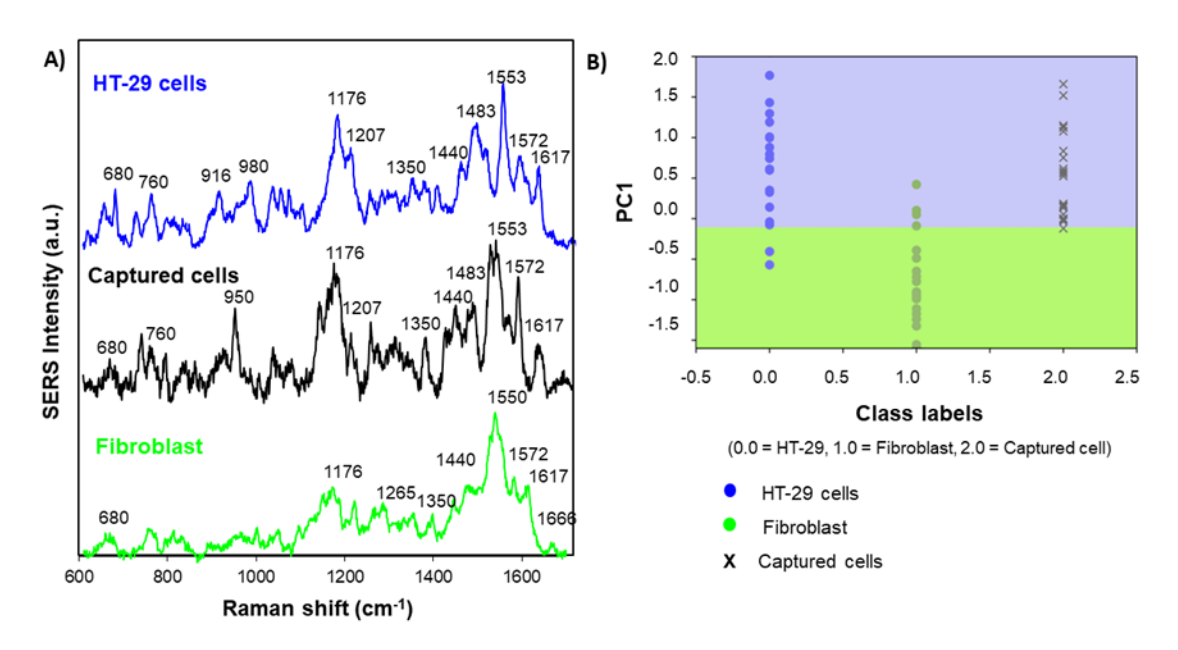


Figure 7. Mean SERS spectra and PCA of the related SERS spectral data. (A) SERS spectra acquired from HT-29 cells, fibroblast, and the captured cells from mixtures. (B) Scatter plots of the scores from the first principal component (PC 1) of the SERS spectra from HT-29 (blue), fibroblast (green), and the captured cells (black).

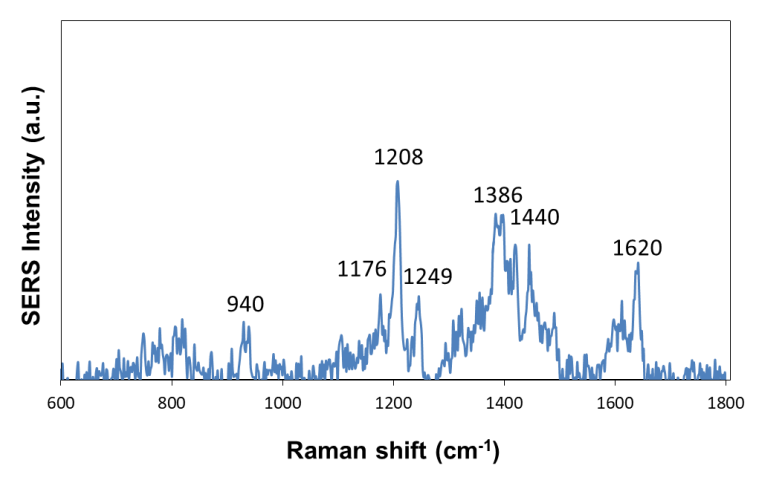


Figure 8. SERS spectrum of immunomagnetic conjugates on the plasmonic paper

In addition, detection of cancerous cells spiked in RBCs was demonstrated to represent the diagnosis of circulating tumor cells (CTCs) that is presented rarely in blood. Different amounts of HT-29 cells including 1000, 5000 and 10000 cells were spiked into 0.1% RBC (approximately 4.133×10^6 cells/mL by counting) independently followed by addition of 10 μ g/mL immunomagnetic conjugates. The results demonstrated that cells were captured from the samples under the magnetic field with high percentage of 94.40%, 88.00%, and 83.09% from 1000, 5000, and 10000 spiked HT-29 cells, respectively (Table 6). The results of target cell enrichment from different

interferences (fibroblasts and RBCs) indicate high capture efficiency of immunomagnetic conjugates toward HT-29 cells in complex conditions. Moreover, the target cells can be simply separated from samples for further detection in less than 30 min. Figure 9A illustrates the mean SERS spectra of the HT-29, RBCs, and the captured cells. The average SERS fingerprint of the captured cells showed strong vibrational bands of amino acid, 1176 cm⁻¹ (C-H) and 1553 cm⁻¹ (N-H), and DNA, 1572 cm⁻¹ (C-C), indicating high amount of protein and nucleic acid corresponding to cancerous cells. In addition, the bands related to porphyrin structure at 754 cm⁻¹ (ring breathing) and 1582 cm⁻¹ (C-C) were relatively weak compared with spectra of single RBC sample. The PCA analysis combined with k-NN algorithm was again performed to analyze HT-29 and RBCs SERS spectra using dominant Raman shifts including 754, 980, 1176, 1207, 1367, 1440, 1553, 1572, 1582, and 1617 cm⁻¹ as depicted in Figure 9A. The PCA plots (Figure 9B) calculated from characteristic peak positions of HT-29 cells and RBCs were clearly differentiated with the sensitivity of 96.4% and specificity of 100%, indicating distinctive SERS spectra between cancerous cells and RBCs. The captured cells were then identified as the cancerous cells (HT-29) with the accuracy of 98.2% using a combination of PCA and k-NN classifier similar to the previous system. Thus, we clearly demonstrated that the paper-based SERS platform with the assistance of immunomagnetic conjugates and multivariate analysis could be applied for cancer cell screening using a simple process and short time. This is comparable with other approaches that have been developed for intrinsic SERS detection of cancer. However, this platform offers significant advancement over previous platforms in minimizing complexity of SERS spectra from interferences by target cell separation process based on bio-recognition interaction between immunomagnetic conjugates and the target cells. This approach couples the sensitivity of SERS technique and specificity derived from magnetic separation that could get rid of non-target cells or other molecules contaminated in biological samples. Moreover, multivariate analysis applied in this platform facilitates the interpretation of SERS spectra and makes cancer cell identification more reliable.

Table 6. Percentage of the captured cells using immunomagnetic conjugate from mixed HT-29 cells and 0.1% RBCs (n = 6)

Number of HT-29 cells	Number of captured cells	% capture
in 0.1% RBCs		
1,000	944	94.40
5,000	4,400	88.00
10,000	8,309	83.09

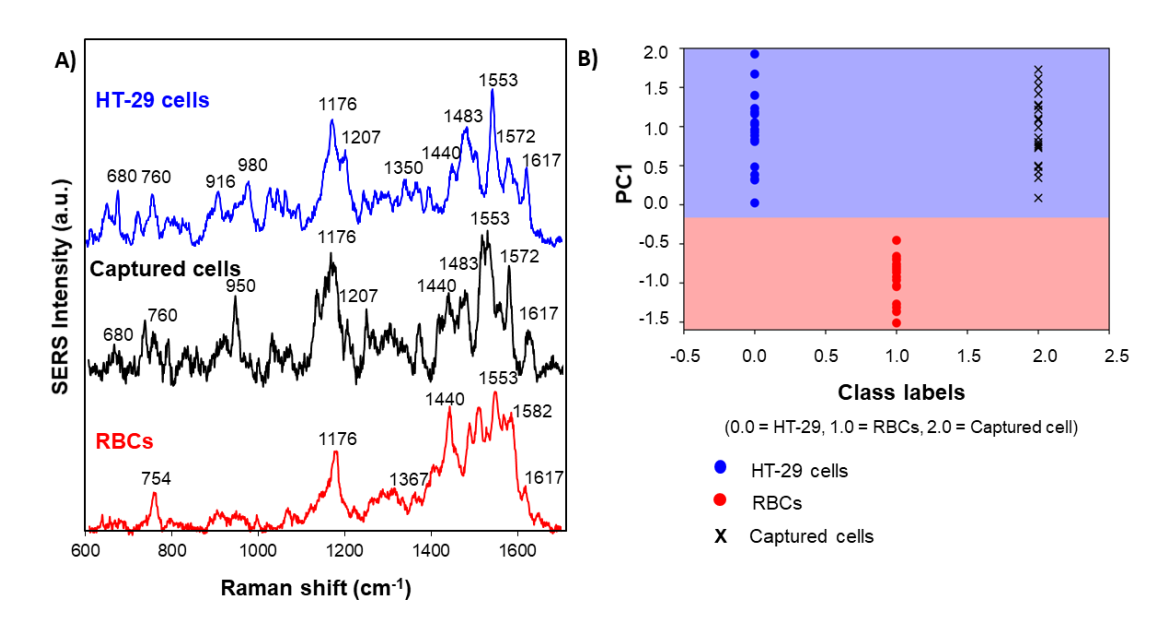


Figure 9. Mean SERS spectra and PCA of the corresponding SERS spectral data. (A) SERS spectra obtained from HT-29 cells, RBCs, and the captured cells from mixtures. (B) Scatter plots of the scores from the first principal component (PC 1) of the SERS spectra from HT-29 (blue), RBCs (red), and the captured cells (black).

2. Detection of miRNA-29a, a biomarker of cervical cancer, using SERs tag

The SERS-based miRNA analysis platform was schematically illustrated in Figure 10. The detection of the target miRNAs was conducted by adding magnetic nanoparticles functionalized with DNA probe into the sample containing the target miRNAs. The magnetic nanoparticles conjugated with DNA probes complementary to 11 bases at the 5'end of the miRNA-29a as demonstrated in Table 1 were acted as capture probes to separated and concentrate the target miRNAs from the sample. Then, SERS tags which were AuNRs functionalized with 4-MBA and DNA probes complementary to 11 bases at the 3' end of the target miRNA sequence were added to the separated samples. In the presence of the target miRNAs, the SERS tags hybridized with the captured target miRNAs and sandwich complexes of MNP-miRNA-SERS tag were formed. The measurement of SERS spectra was then performed to determine the presence of the target miRNAs.

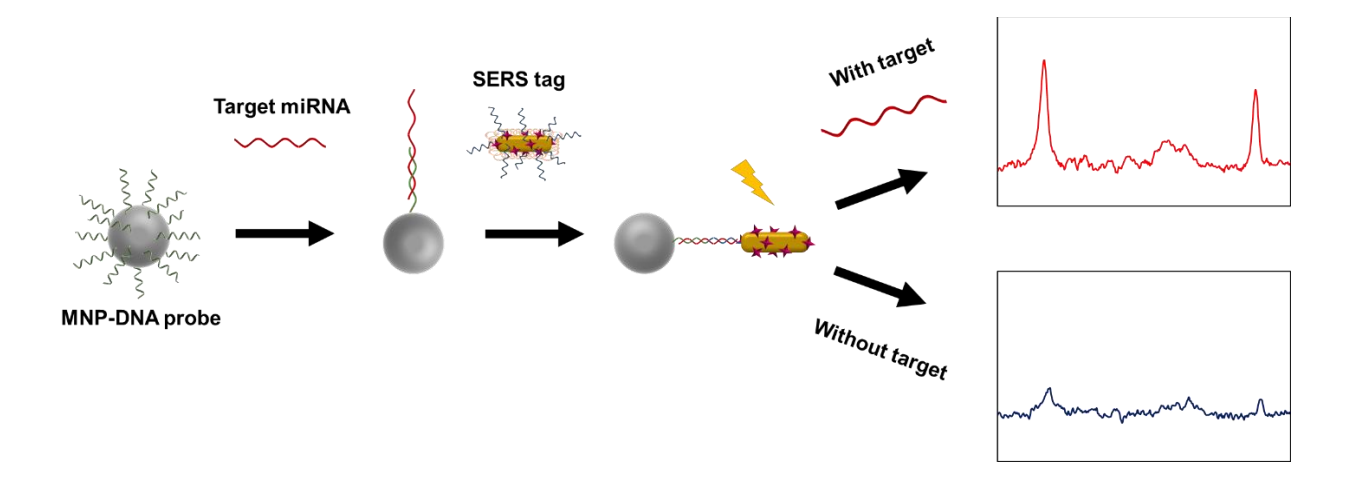


Figure 10. Schematic illustration of miRNA detection of miRNA using SERS tags and magnetic conjugated DNA probes.

2.1 Preparation and Characterization of SERS tags and capture probes

First, the AuNRs were synthesized by a modified seed-mediated growth method using CTAB as a building block as described previously. The characteristic UV-Vis spectrum and TEM image of the synthesized AuNRs were confirmed in Figure 11. The TEM image demonstrated that the synthesized AuNRs had the aspect ratio of 2.76, with the average width of 17±2 nm and the average length of 47±2 nm, respectively. Additionally, UV-Vis absorption revealed that the synthesized AuNRs had a weak plasmon band at 516 nm and a strong longitudinal band at 708 nm.

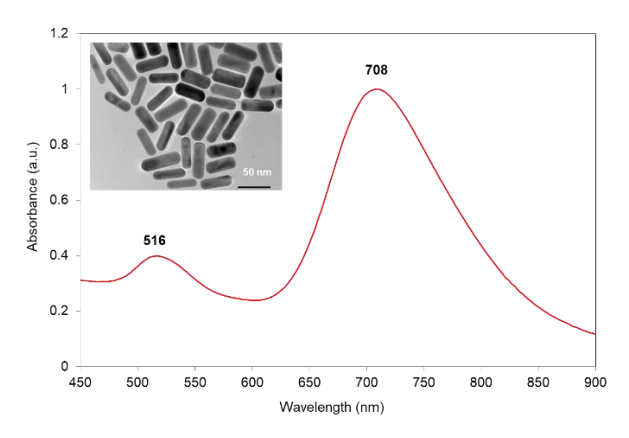


Figure 11. The characteristic UV-Vis spectrum and TEM image of the AuNRs.

Then, the SERS tags were prepared using layer-by-layer process as schematically illustrated in Figure 12. The Raman reporters, 4-MBA, were absorbed on the surface of the as-prepared AuNRs through thiol-gold interaction. For this experiment, synthetic thiolated DNA probes (P1) specific to one end of the target miRNA-29a sequence as shown in Table 1 were conjugated to the 4-MBA-AuNRs through thiol-gold interaction to form SERS tags. Additionally, a monolayer of PEG was added to the AuNRs surface to stabilize and minimize aggregation of the SERS tags.

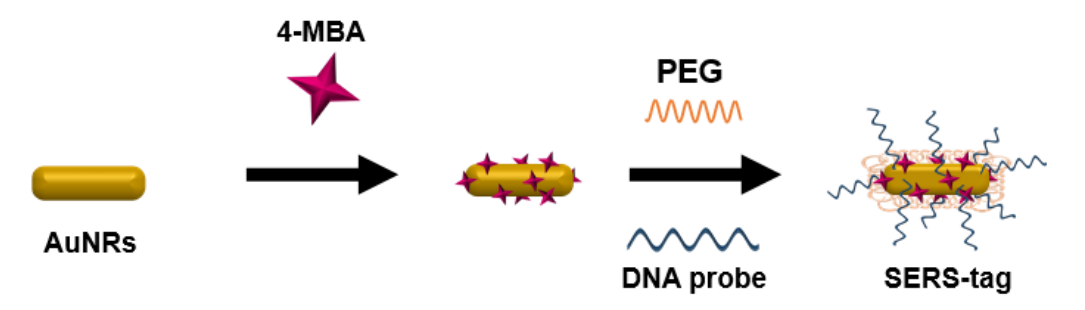


Figure 12. Preparation of SERS tag by layer-by-layer process using AuNRs conjugating with 4-MBA followed by addition PEG and DNA probe complementary to the target miRNA.

After fabrication, the signal of SERS tags was then determined by using a Raman spectrometer with an excitation laser at 785 nm. As showed in **Figure 13**, the SERS tag showed strong characteristic peaks at 1077 and 1586 cm⁻¹ which derived from a v(C-S) stretching vibration and to a v(C-C) aromatic ring vibration of 4-MBA, respectively [32], while the AuNRs did not showed any SERs spectra. This confirmed that 4-MBA was attached firmly on AuNRs surface and the signal was greatly enhanced by electromagnetic field from AuNRS.

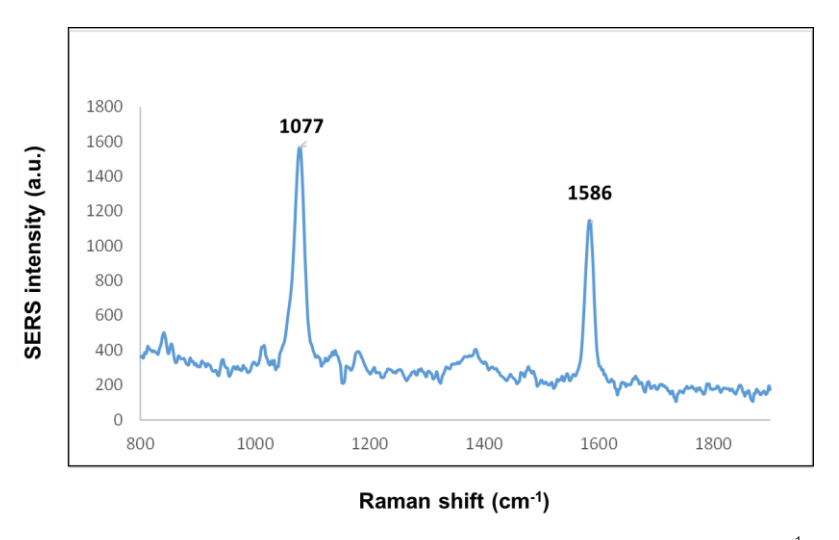


Figure 13. Spectra of SERS tag showed characteristic peak of 4-MBA at 1077 and 1586 cm⁻¹

The capture probes were prepared by conjugation of amine-modified DNA probes specific to the target miRNA-29a (P2) to the surface of carboxylated magnetic nanoparticles (MNPs) through EDC/NHS coupling as described in the experimental section. The changes in the hydrodynamic size and zeta potential of the magnetic nanoparticles before and after conjugation were then determined. The hydrodynamic size of the unmodified MNPs and MNP-DNA probes were 151.7 nm and 211.0 nm, respectively. Moreover, the zeta potentials of the carboxylated MNP and that of MNP-DNA probes were slightly change from -15.43 mV and -11.7 mV which confirm successful immobilization of the DNA probes.

2.2 SERS-based miRNA detection

Here, the detection of the target miRNA was demonstrated using SERS tags with the assist of magnetic nanoparticles for target capture and separation. By applying magnetic conjugates to the samples containing the target, the miRNA-29a was captured by the MNP-DNA probes specific to the target and then labeled with the SERS tags to form sandwich complexes. The complexes were then separated from the samples by an external magnet for SERS measurement. In the absence of target, the SERS tags were washed away, hence, no SERS signal was observed (Figure 14).

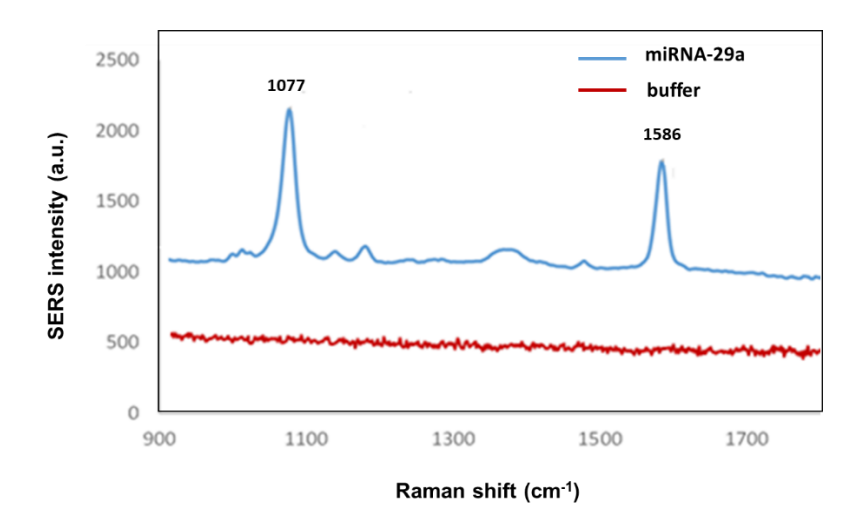


Figure 14. SERS spectra of the samples in the presence and absence of the target miRNA-29a.

To evaluate the detection sensitivity of the system, different concentrations of target miRNA-29a ranging from 0-1000 pM were spiked in buffer. Based on SERS spectra in Figure 15A, it can be observed that the intensity of the 4-MBA characteristic peaks from SERS tags proportionally increased when the concentration of the target miR-29a was raised. The quantitative analysis of the system was also conducted by considering the Raman shift at 1077 and 1586 cm⁻¹. The relative Raman intensity was then plotted as a function of miRNA-29a concentration as shown in Figure 15B. The limit of detection (LOD) was then approximated to be 10 pM.

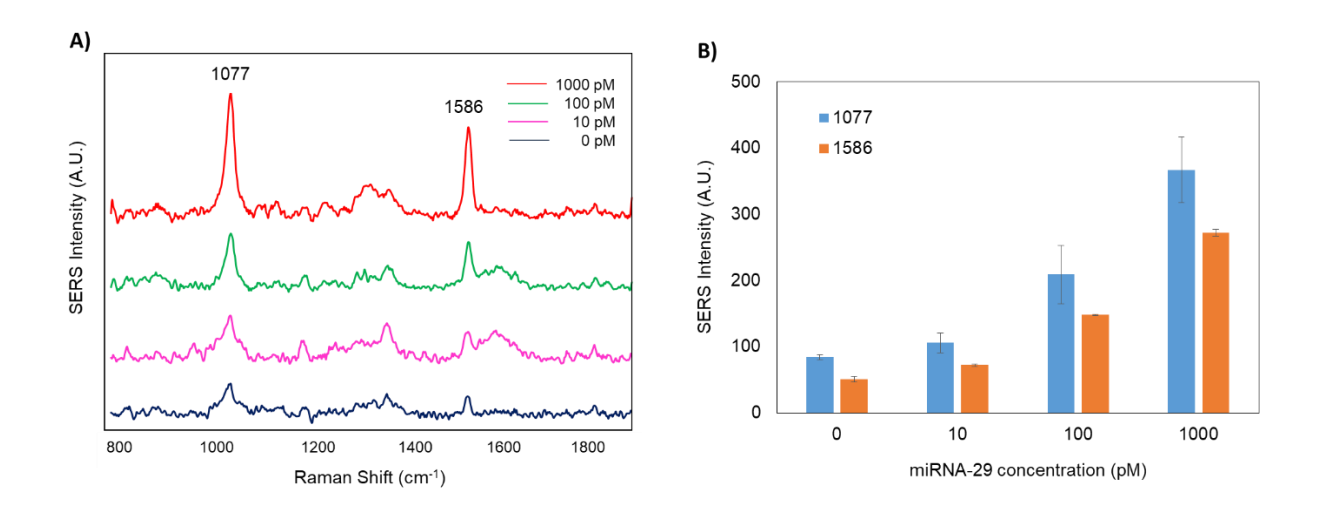


Figure 15. Sensitivity evaluation using various concentration of miRNA-29a from 0-1000 pM. (A) SERS spectra obtained from individual samples (B) Quantitative analysis of miRNA-29a by observing SERS intensity at 1077 and 1586 cm⁻¹.

2.2 Specificity of the system

The specificity of the system was assessed using the target miRNA-29a 100 pM compared to non-targets including miRNA-21 and miRNA-210. The Raman shift intensity at 1077 and 1586 cm⁻¹ after background (signal from buffer) subtraction were plotted as shown in **Figure 16**. Strong SERS signal at both 1077 and 1586 cm⁻¹ was observed for the positive sample, whereas negative samples yielded very low signal. This results indicated high specificity of the system toward the target miRNA-29a and low non-specific interaction with other non-target miRNA.

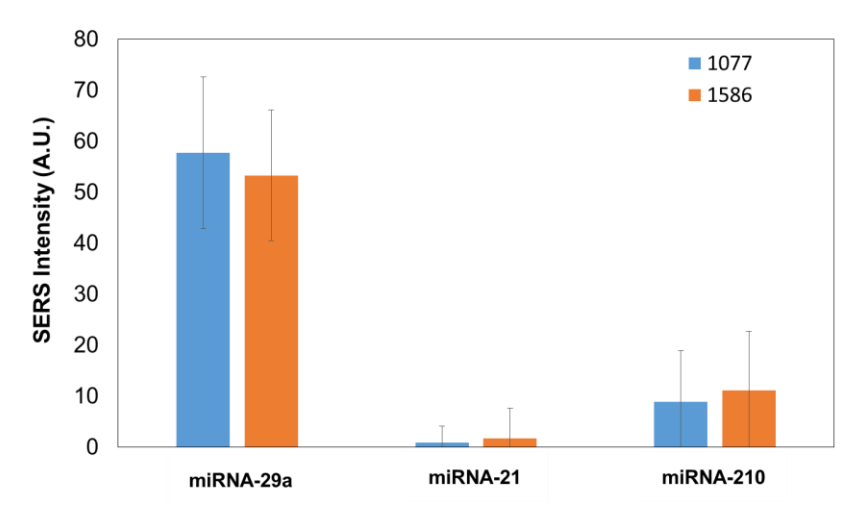


Figure 16. Specificity of the system was evaluated using the target miRNA-29a

Conclusion

In the first part of this project, a system of paper-based SERS substrate combined with magnetic separation was developed for simple and effective cancer screening. Distinguished SERS spectra of colon cancer cells, normal cells, and RBCs could be achieved, reflecting diverse levels of proteins, nucleic acids, and lipids due to structural and metabolic changes. By applying immunomagnetic conjugates, the target cells were concentrated and separated from cell mixtures with high percentage of 80-90% through specific recognition between antibodies and biomarkers overexpressed on the surface of cancer cells. Based on PCA analysis and k-NN algorithm, each cell type could be differentiated with high sensitivity and specificity. Additionally, the captured cells could be verified and identified as cancerous cells (HT-29) with high accuracy up to 98%. Our results demonstrate that the plasmonic paper with the assistance of magnetic separation and multivariate analysis provides a convenient, rapid, and costeffective system for colon cancer cell detection, which can potentially be applied for screening other cancer cells or biomarkers.

Additionally, we developed SERS tags using AuNRs functionalized with Raman reporters and DNA probes using layer-by-layer process for the detection of target miRNA-29a which is biomarker of cervical cancer. The magnetic conjugated DNA probes were applied to capture and separate the target from the samples prior to SERS tags labelling. Significantly, the detection signal was increased proportionally to the concentration of the target. Moreover, the system was found to provide good sensitivity and be able to detect the target in picomolar range. The specificity of the system was also illustrated using other non-target miRNAs. This study demonstrated that the SERS tags with the assist of magnetic conjugated DNA probes could be used for target miRNA analysis, which possibly be applied for other cancer biomarkers detection.

References

- [1] Doering WE, Piotti ME, Natan MJ, Freeman RG. SERS as a Foundation for Nanoscale, Optically Detected Biological Labels. Adv. Mater. 19: 3100-3108 (2007)
- [2] Kumar GVP. Plasmonic nano-architectures for surface enhanced Raman scattering: a review. J. Nanophotonics. 6: 64503(1-20) (2012)
- [3] Nikoobakht B, El-Sayed MA. Preparation and growth mechanism of gold nanorods (NRs) using seed-mediated growth method. Chem. Mater. 15: 1957-1962 (2003)
- [4] Tripp RA, Dluhy Richard A. Zhao Y. Novel nanostructures for SERS biosensing. Nanotoday 3: 31-37 (2008)
- [5] Stewart ME, Anderton CR, Thompson LB, et al. Nanostructured Plasmonic Sensors. Chem. Rev. 108: 494–521 (2008)
- [6] Banholzer MJ, Millstone JE, Qina L. Rationally designed nanostructures for surface-enhanced Raman spectroscopy. Chem. Soc. Rev. 37: 885–897 (2008)

- [7] Wang Y, Yan B, Chen L. SERS Tags: Novel optical nanoprobes for bioanalysis. Chem. Rev. 113: 1391-1428 (2013)
- [8] Dong H, Lei J, Ding L, et al. MicroRNA: function, detection, and bioanalysis. Chem. Rev. 113: 6207-6233 (2013)
- [9] Mishra PJ. MicroRNAs as promising biomarkers in cancer diagnostics Biomarker Research 2:19(1-4) (2014)
- [10] Bertoli G, Cava C, Castiglioni I. MicroRNAs: New biomarkers for diagnosis, prognosis, therapy prediction and therapeutic tools for breast cancer. Theranostics 5:10 1122-1143 (2015)
- [11] Huang YF, Sefah K, Bamrungsap S, et al. Selective photothermal therapy for mixed cancer cells using aptamer-conjugated nanorods. Langmuir 24: 11860-11865 (2008)
- [12] Lee CH, Tian L, Singamaneni S. Paper-based SERS swab for rapid trace detection on real-world surfaces, ACS Appl. Mater. Interfaces 2: 3429–3435 (2010)
- [13] Lee CH, Hankus ME, Tian L, Pellegrino PM, Singamaneni S. Highly sensitive surface enhanced Raman scattering substrates based on filter paper loaded with plasmonic nanostructures, Anal. Chem. 83: 8953–8958 (2011)
- [14] Yu WW, White IM. Inkjet-printed paper-based SERS dipsticks and swabs for trace chemical detection, Analyst 138: 1020–1025 (2013)
- [15] Satheeshkumar E, Karuppaiya P, Sivashanmugan K, Chao WT, Tsay HS, Yoshimura M. Biocompatible 3D SERS substrate for trace detection of amino acids and melamine, Spectrochim. Acta A Mol. Biomol. Spectrosc. 181: 91–97 (2017)
- [16] Ghosh SK, Pal T. Interparticle coupling effect on the surface plasmon resonance of gold nanoparticles: from theory to applications, Chem Rev. 107: 4797–4862 (2007)
- [17] Kelly KL, Coronado E, Zhao LL, Schatz GC. The optical properties of metal nanoparticles: the influence of size, shape, and dielectric environment, J. Phys. Chem. B 107: 668–677(2003)
- [18] Zhu S, Fan C, Wang J, He J, Liang E. Surface-enhanced Raman scattering of 4-mercaptobenzoic acid and hemoglobin adsorbed on self-assembled Ag monolayer films with different shapes, Appl. Phys. A 117: 1076–1083 (2014)
- [19] Kim WS, Shin JH, Park HK, Choi S. A low-cost, monometallic, surface-enhanced Raman scattering-functionalized paper platform for spot-on bioassays, Sens. Actuators B Chem. 222: 1112–1118 (2016)
- [20] Hasi WLJ, Lin S, Lin X, Lou XT, Yang F, Lin DY, Lu ZW. Rapid fabrication of self-assembled interfacial film decorated filter paper as an excellent surface-enhanced Raman scattering substrate, Anal. Methods 24: 9547–9553 (2014)
- [21] Hou M, Huang Y, Ma L, Zhang Z. Quantitative analysis of single and mix food antiseptics basing on SERS spectra with PLSR method, Nanoscale Res. Lett. 11: 296 (2016)

- [22] Liu Q, Wang J, Wang B, Li Z, Huang H, Li C, Yu X, Chu PK. Paper-based plasmonic platform for sensitive, noninvasive, and rapid cancer screening, Biosens. Bioelectron. 54: 128–134 (2014)
- [23] Notingher I, Hench LL. Raman microspectroscopy: a noninvasive tool for studies of individual living cells in vitro, Expert Rev. Med. Devices 3: 215–234 (2006)
- [24] Girish CM, Iyer S, Thankappan K, Rani VVD, Gowd GS, Menon D, Nair S, Koyakutty M. Rapid detection of oral cancer using Ag-TiO₂ nanostructured surface-enhanced Raman spectroscopic substrates, J. Mater. Chem. B 2: 989–998 (2014)
- [25] Terentis AC, Fox SA, Friedman SJ, Spencer ES. Confocal Raman microspectroscopy discriminates live human metastatic melanoma and skin fibroblast cells, J. Raman Spectrosc. 44: 1205–1216 (2013)
- [26] Votteler M, Berrio DAC, Pudlas M, Walles H, Schenke-Layland K. Non-contact, label-free monitoring of cells and extracellular matrix using Raman spectroscopy, J Vis. Exp. 63: e3977 (2012)
- [27] Premasiri WR, Lee JC, Ziegler LD. Surface-enhanced Raman scattering of whole human blood, blood plasma, and red blood cells: cellular processes and bioanalytical sensing, J. Phys. Chem. B 116: 9376–9386 (2012)
- [28] Shao J, Yao H, Meng L, Li Y, Lin M, Li X, Liu J, Liang J. Raman spectroscopy of circulating single red blood cells in microvessels in vivo, Vib. Spectrosc. 63: 367–370 (2012)
- [29] Zhang S, Tian X, Yin J, Liu Y, Dong Z, Sun JL, Ma W. Rapid, controllable growth of silver nanostructured surface-enhanced Raman scattering substrates for red blood cell detection, Sci. Rep. 6: 24503 (2016)
- [30] Huang YY, Li N, Zhou SN, Huang ZT, Zhuang ZF. Study of hemoglobin response to mid-ultraviolet (UVB) radiation using micro-Raman spectroscopy. Appl. Phys. B 123: 237 (2017)
- [31] Safarik I, Safarikova M. Magnetic techniques for the isolation and purification of proteins and peptides, Biomagn. Res. Technol. 2: 7 (2004)
- [32] Michota A, Bukowska J. Surface-enhanced Raman scattering (SERS) of 4-mercaptobenzoic acid on silver and gold substrates, J. Raman Spectrosc. 34: 21–25 (2003)

FISEVIER

Contents lists available at ScienceDirect

Sensors and Actuators B: Chemical

journal homepage: www.elsevier.com/locate/snb



A simple paper-based surface enhanced Raman scattering (SERS) platform and magnetic separation for cancer screening



Pimporn Reokrungruang^{a,b}, Itthi Chatnuntawech^a, Tararaj Dharakul^{b,*}, Suwussa Bamrungsap^{a,*}

- ^a National Nanotechnology Center, National Science and Technology Development Agency, Thailand Science Park, Pahonyothin Road, Khlong Nueng, Khlong Luang, Pathum Thani, 12120, Thailand
- b Department of Immunology, Faculty of Medicine Siriraj Hospital Mahidol University, Wanglang Road, Bangkoknoi, Bangkok, 10700, Thailand

ARTICLE INFO

Keywords: Surface enhanced Raman scattering (SERS) Plasmonic paper Gold nanorod Magnetic separation Cancer screening

ABSTRACT

Early and precise diagnosis of cancer is critical for a better prognosis. Here, we describe a simple and costeffective plasmonic paper as a surface enhanced Raman scattering (SERS) substrate in combination with magnetic separation for cancer screening. The plasmonic paper was fabricated by immersing plain filter paper into gold nanorod solution and the SERS property of the paper was evaluated using 4-mercaptobenzoic acid (4-MBA) and rhodamine 6 G (R6 G), which showed an enhancement factor (EF) in the range of 106-108. HT-29, a colorectal cancer cell line that highly expresses epithelial cell adhesion molecule (EpCAM), served as the target cells; non-EpCAM-expressing cells, namely fibroblasts and red blood cells (RBCs), were used as negative controls. Intrinsic SERS spectra of the target and control cells showed distinctive patterns on the plasmonic paper due to differences in their structure and components. A combination of principal component analysis (PCA) and knearest-neighbor algorithm (k-NN) was employed to analyze and distinguish the acquired HT-29 and fibroblast SERS spectra, demonstrating a diagnostic sensitivity and specificity of 84.8% and 82.6%, respectively, whereas the differentiation between HT-29 and RBCs SERS spectra showed a sensitivity and specificity of 96.4% and 100%, respectively. The magnetic separation was applied to capture the target cells from cell mixtures followed by PCA and k-NN analysis. The identification of the captured cells as cancerous cells from the HT-29 and fibroblast mixture indicated an accuracy of 83.7%, while that from a mixture of HT-29 and RBCs was 98.2%. Thus, the simple paper-based SERS substrate with the assistance of magnetic enrichment and multivariate analysis offers a potent new platform for cancer cell detection and screening.

1. Introduction

The early and precise diagnosis of cancer can increase chances of a successful treatment and improve survival rates of the cancer patients. Therefore, there is a high demand for the development of novel diagnostic tools for cancer screening having high sensitivity and specificity. Owing to the advance in nanotechnology, nanomaterial-based platforms together with optical measurement techniques including fluorescence, surface plasmon resonance (SPR), and colorimetry, have been employed for cancer detection [1]. Surface enhanced Raman scattering (SERS) has become an important tool for detection of specific biomolecules in recent years due to its advantage of high sensitivity at the single molecule level [2]. The unique Raman spectra, defined as the "fingerprint", of particular molecules provide the identification and quantitation of specific targets. Moreover, SERS can be utilized for multiplex detection due to its high spatial resolution and utilization of a

single wavelength excitation.

In SERS-based detection, enhancement can be achieved when target analytes are absorbed or located on a "SERS substrate" in close proximity within a 10 to 100 nm scale [2]. A number of SERS substrates including roughened noble metal surfaces and patterned metal nanostructures with enhancement factors ranging from 10⁴ to 10¹⁰ have been demonstrated [3]. To fabricate SERS substrate, several techniques which are both top-down and bottom-up approaches have been applied such as e-beam lithography, colloidal lithography, on-wire lithography, including self- and directed-assembly, which enable precise control over the size, shape, and organization of the metal nanostructures [4]. However, preparation of SERS substrates using these techniques is time consuming, expensive, and requires sophisticated equipment. Therefore, the development of simple, cost-effective, and scalable SERS substrates is highly desirable.

Recently, plasmonic paper, which is paper coated with metallic

E-mail addresses: tararaj.dha@mahidol.ac.th (T. Dharakul), suwussa@nanotec.or.th (S. Bamrungsap).

^{*} Corresponding authors.

nanostructures, has been fabricated and reported as an effective SERS substrate [5,6]. Paper-based biosensors provide advantages of being cost-effective, mechanically favorable (easy to cut or shape), and easily disposable [7]. The porous structure of paper also provides large surface area suitable for high amount of nanoparticle absorption compared with flat non-porous surfaces. Moreover, paper can act as microfluidics for liquid sample transportation and the analytes can be concentrated at specific area by solvent evaporation [8]. Recently, there has been a growing interest in applying paper based-SERS substrate for detection of trace chemicals and bioanalysis. A paper coated with silver nanoparticles (AgNPs) was demonstrated to detect explosives, pesticides, and narcotics drugs with high sensitivity at nanogram range [9.10]. Lately, paper-based SERS substrates have been applied in cancer detection; for example, Kim and coworkers reported the use of AgNPpaper as a SERS substrate for the detection of cervical fluids for human papillomavirus (HPV) infection associated with cervical cancer [11]. With specific fingerprint resulting from different components, normal and infected fluid could be differentiated as well as specific type of HPV infection could be identified. Another study reported the use of paper substrate for oral cancer detection using gold nanorods (AuNRs) coated on filter paper as a scaffold. Different SERS spectra obtained from normal and cancerous cells due to specific biomolecular changes were observed. By comparing the peak densities, cells exfoliated from cancerous and normal tissues could be distinguished with a sensitivity and specificity up to 70-100% [12].

Here, we demonstrated a system of plasmonic paper as SERS substrate combined with magnetic separation for cancer cell screening as depicted in Scheme 1. The plasmonic paper was simply fabricated by dipping plain filter paper into AuNR solution. AuNR was selected as a plasmonic material due to its strong extinction coefficient, tunable longitudinal SPR band ranging from visible to near-infrared region, and high stability [13]. Colorectal cancer cells (HT-29) with over expressed EpCAM were chosen as a model of target cells, while normal cells (fibroblasts) and RBCs were used as controls. Magnetic separation was performed to separate and enrich the target cancer cells from the mixtures to reduce background and interference using specific recognition between immunomagnetic conjugate and the target cells. The intrinsic SERS spectra of the HT-29 cells, fibroblasts, RBCs, and the enriched cells were achieved with signal enhancement on the plasmonic

paper. The HT-29 enriched cells were identified based on distinctive SERS pattern of cancerous cells compared with those of fibroblasts and RBCs with the assistance of multivariate analysis.

2. Materials and methods

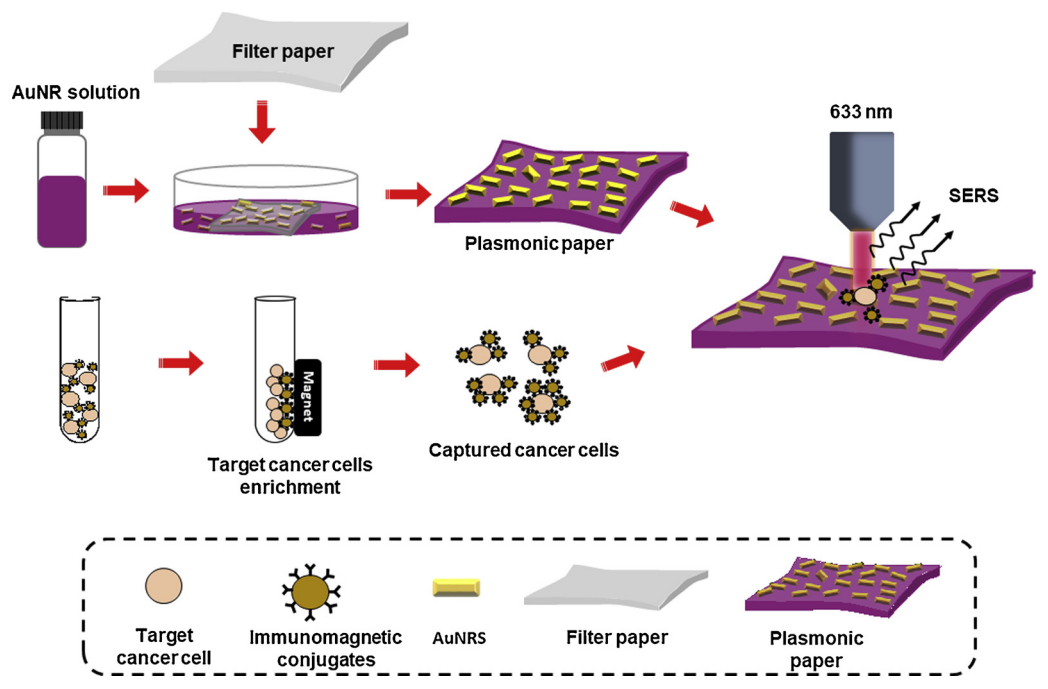
2.1. Materials

Hexadecyltrimethylammonium bromide (CTAB), chloroauric acid (HAuCl $_4$ ·4H $_2$ O), sodium borohydride (NaBH $_4$), silver nitrate (AgNO $_3$), L-ascorbic acid (C $_6$ H $_8$ O $_6$), glycine, (N-Ethyl-N-(3-dimethylaminopropyl) carbodiimide hydrochloride (EDC), N-hydroxysulfosuccinimide sodium salt (NHS), 4-mercaptobenzoic acid (4-MBA), and rhodamine 6 G (R6 G) were purchased from Sigma-Aldrich, USA. Filter paper was supplied from Whatman no. 1, UK. McCoy's 5 A Medium and Dulbecco's Modified Eagle Medium (DMEM) was purchased from Gibco, USA. Magnetic particles were supplied by Dynabeads, Invitrogen, USA. EpCAM-specific antibody (VU-1D9) was purchased from Sigma, USA.

2.2. Plasmonic paper preparation

AuNRs were synthesized based on a modified seed-mediated growth method using CTAB as the template as described in previous studies [13,14]. After synthesis, the AuNRs were washed three times by centrifugation at 12,000 rpm for 8 min at 25 °C to remove excess chemicals. The AuNRs were then characterized by UV-VIS absorption (Power wave XS2, Bio-Tek, USA) and transmission electron microscope (TEM, JEM 2100, JEOL, Japan).

The plasmonic paper was prepared by immobilization of AuNRs on laboratory filter paper. The filter paper was cut to $1\times 1~{\rm cm}^2$ and immersed into petri dish containing AuNR solution at room temperature overnight. The plasmonic paper was rinsed with deionized water and dried at 37 °C for 30 min. The immersing process was repeated again and then the plasmonic paper was kept at 35% relative humidity before use. The distribution of AuNRs on the paper substrate was examined through scanning electron microscope (SEM) using FE-SEM SU8030 (Hitachi, Japan) at acceleration voltage of 5.0 kV. To evaluate the Raman enhancement property, the plasmonic paper was dipped in different concentrations of 4-MBA solution for 30 min and dried for



Scheme 1. Schematic diagram illustrating the plasmonic paper fabrication and cancer cell detection with the assistance of magnetic enrichment.

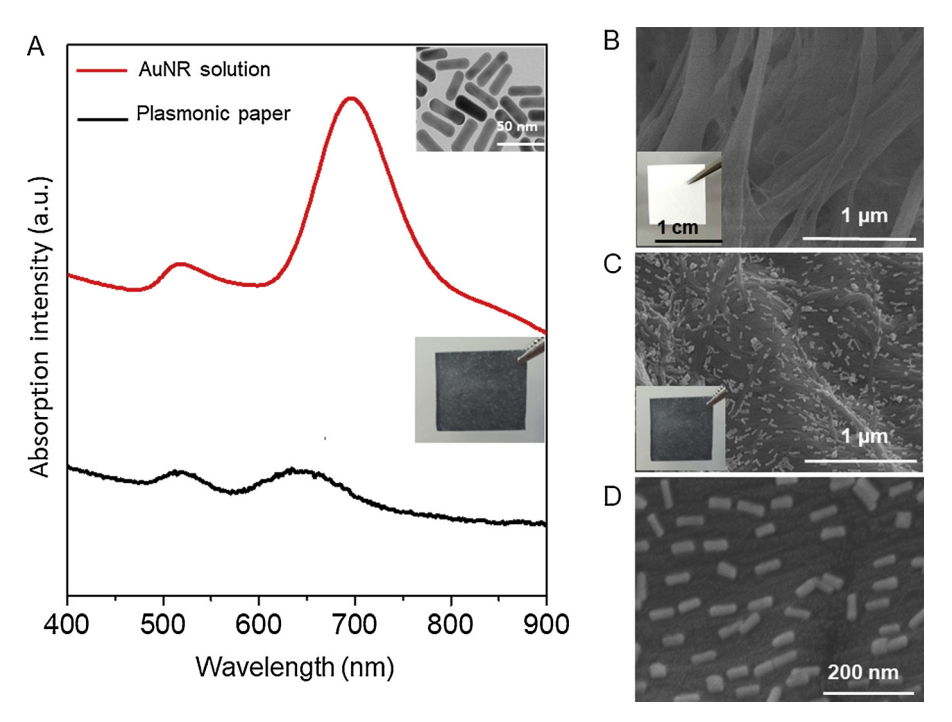


Fig. 1. Characterization of AuNRs and plasmonic paper. (A) Absorption spectra of AuNR solution and the plasmonic paper. (B) SEM image of bare filter paper. (C–D) SEM images of the plasmonic paper (AuNR coated).

30 min under 37 °C. SERS measurement was performed using a Raman spectrometer (NT-MDT, Russia) coupled with an inverted confocal microscope (Olympus IX71, Olympus, USA). A He-Ne laser at wavelength of 633 nm through $100\times$ objective lens with power of 3.3 mW was utilized to excite samples. The exposure time was $10 \, \mathrm{s}$ with 5 accumulations and the detection range was $100\text{-}1900 \, \mathrm{cm}^{-1}$. SERS spectra from five different locations were collected for each concentration of 4-MBA and the SERS intensities were averaged for enhancement factor calculation.

2.3. Cell culture

Human colorectal adenocarcinoma cancer (HT-29) cell line was cultured with McCoy's 5 A medium supplemented with 10% fetal bovine serum, penicillin (10,000 units/mL), and streptomycin (10 mg/mL). Fibroblast that does not express EpCAM was cultured in DMEM supplemented with 10% fetal bovine serum, penicillin (10,000 units/mL), and streptomycin (10,000 µg/mL). Both cell lines were cultured in humidified atmosphere at 37 °C with 5% CO $_2$. Before performing experiments, cells were harvested by trypsinization, washed and re-suspended in 10 mM phosphate buffered saline (PBS). The number of cells was counted using a hemocytometer through an inverted microscope (Olympus CKX41, USA).

2.4. Immunomagnetic conjugate preparation

To prepare immunomagnetic conjugate, 0.1 mg of 1 μ m carboxy-lated magnetic particles was suspended in 15 mM MES buffer (pH 6.0). Then 0.1 mg EDC and 0.2 mg NHS was added to activate carboxyl groups on the magnetic beads to form active esters. The activated magnetic beads were then exchanged into PBS (pH 7.4) and incubated with 5 μ g EpCAM-specific antibody for 3 h on ice. Excess antibodies and reagents were removed by magnetic separation using a magnet attached to the side of Eppendorf tube followed by removal of supernatant liquid. Then, the immunomagnetic conjugate was washed twice and kept in PBS containing 0.1% Tween-20 and 0.1% bovine serum albumin (BSA) at 4 °C. The immunomagnetic conjugate was characterized by dynamic light scattering and zeta potential using Zeta

Nanosizer (Malvern Instruments, UK) with 10 kV backscattered-electron mode (BSE).

2.5. Cancer cell detection in mixture samples

Five thousand HT-29 cells were mixed with fibroblasts at different ratios including 1:1 (5000:5000), 1:2 (5000:10,000), and 1:5 (5000:25,000) HT-29:fibroblast, respectively. The immunomagnetic conjugate at a concentration of 10 µg/mL was incubated with the samples on ice for 30 min A magnet was applied to the samples for 5 min followed by supernatant liquid removal to separate unbound cells. The separation was processed thrice for each sample and the captured cells were then re-suspended in 30 µL of 10 mM PBS for counting under a microscope. Five microliters of the captured cells were dropped on a plasmonic paper and dried for 30 min. SERS spectra of cells deposited on the plasmonic paper were obtained using the laser power of 0.17 mW and exposure time of 20 s with 3 accumulations. The SERS spectra of 20 samples (n = 20) from each cell type with different locations from each sample were collected in the range of 100-1900 cm⁻¹ and baseline subtraction was performed by the software package WIRE 4.2 (Renishaw). To imitate the detection of circulating tumors, different number of HT-29 cells (1000, 5000, and 10,000 cells) were spiked in 0.1% RBCs in 10 mM PBS ($^{\sim}4.113 \times 10^6$ cells/mL) independently. The immunomagnetic conjugate was then applied to the samples for target cells enrichment and SERS spectra of the enriched cells were examined similar to the previous experiments. A combination of principal component analysis (PCA) and k-nearest-neighbor algorithm (k-NN) was performed on 20 different data sets for each cell type including the enriched cells for comparison and identification using scikit-learn software.

3. Results and discussion

3.1. Plasmonic paper fabrication and characterization

The plasmonic paper was fabricated starting with AuNR synthesis by seed mediated growth method using CTAB as a surfactant. As shown in Fig. 1A, the AuNRs presented transverse and longitudinal absorption

bands at 526 and 696 nm, respectively, according to the oscillation of electrons along their facets. The TEM image inset reveals the average width and length of 16 \pm 2 nm and 51 \pm 5 nm with the aspect ratio (length divided by width) of 3.2. To prepare plasmonic paper, laboratory filter paper with the size of 1 × 1 cm² was immersed into AuNR solution overnight twice. After immersing, a dark red-purple color was observed from the paper indicating successful loading of the AuNRs on the paper. Surface plasmon resonance (SPR) absorption of the plasmonic paper was observed with blue shift and broader bands compared with that of the AuNR solution as shown in Fig. 1A. This change is due to the alteration of dielectric ambient after loading AuNRs on the paper resulting in the decrease of refractive index [15]. Fig. 1B shows the surface morphology of plain laboratory filter paper including different layers of fiber by SEM image. After coating, AuNRs were distributed throughout the fiber without aggregation as demonstrated in SEM images (Fig. 1C and D). AuNRs were deposited firmly on three dimensional structure of the paper due to electrostatic interaction between the positive charge of CTAB capping AuNRs and the negative charge of the hydroxyl-rich cellulose paper [16]. It was observed that high amount of AuNRs assembled on the paper surface with an approximate number of 188 \pm 20 NPs/ μ m². With high density of AuNRs, intensive electromagnetic field can be produced from several hotspots generated by AuNRs located on the plasmonic paper surface with suitable inter-particle distance [8]. This effect intensifies the local light absorption and scattering, resulting in high signal enhancement ability of the plasmonic paper [17-19].

To evaluate the enhancement property of the plasmonic paper, a typical Raman active molecule, 4-MBA, was loaded on the paper. The plasmonic paper and filter paper were dipped in different concentrations of 4-MBA solution ranging from 0.1 nM to 1 M for 30 min. SERS and Raman spectra of 4-MBA were then obtained from five different random locations on each substrate. The most intense characteristic Raman shift of 4-MBA appearing on the paper at 1590 cm $^{-1}$ was assigned to ring breathing mode of $\nu(\text{C-C})$ [20] and was selected and averaged for EF calculation using following equation, the derivation of which is demonstrated in Supplementary material [21]:

$$EF = \frac{I_{SERS}}{I_{Raman}} \times \frac{C_{Raman}}{C_{SERS}} \tag{1}$$

where I_{SERS} is the SERS intensity of 4-MBA on the plasmonic paper, C_{SERS} is the concentration of 4-MBA on the plasmonic paper, I_{Raman} is the Raman intensity of 4-MBA on a filter paper, and C_{Raman} is the concentration of 4-MBA on a filter paper. Based on SERS intensity at 1590 cm⁻¹, the EF of the plasmonic paper was calculated to be about 10⁷-10⁸ (Table S1) with the detection limit of 1 nM (Fig. 2), which is consistent with other paper-based SERS substrates that were previously reported by other research groups [22,23]. To eliminate the selective enrichment of the analytes on the plasmonic paper due to strong thiolgold affinity between 4-MBA and AuNRs, Rhodamine 6 G (R6 G), which does not have such interaction with the substrate, was also applied. Utilization of R6 G resulted in an EF in the similar range of 10⁶ -10⁷, as demonstrated in Figs. S2, S3, and Table S2. The fabrication of SERS substrate using this technique is not only simple and cost-effective, but the resulting plasmonic paper also shows good enhancement property and feasibility for target analyte detection.

3.2. SERS spectra of cancerous cells, fibroblast, and RBCs

Prior to performing the detection and identification of the target cancer cells from samples, SERS spectra of cancerous cells (HT-29), normal cells (fibroblast), and RBCs were acquired on the plasmonic papers. The cell suspension containing each cell type was dropped and dried on the plasmonic paper. After drying, the cells were dehydrated resulting in membrane damage and cytoskeletal changes. Therefore, we presumed that not the whole cells but fractions of cells likely contacted with the plasmonic paper after cell death. Moreover, some intracellular

components such as DNA fragments from nuclear matrix could have leaked and interacted with the plasmonic paper. As a result, SERS spectra achieved on the plasmonic paper would contain information of biomolecules from both cell surface and intracellular components. As demonstrated in Fig. 3, all cells yielded strong SERS signal demonstrating excellent enhancement performance of the plasmonic paper, with different fingerprints among various cell types corresponding to results achieved in another study [12]. Metabolically active cancer cells are known to produce large amount of protein and nucleic acid, resulting in dominating signature bands of protein components and nucleic acids. Here, the average SERS spectrum of HT-29 cells showed intense bands of protein at 758–760 cm⁻¹ (ring breathing). 1175-1177 cm⁻¹ (C-H), 1207-1209 cm⁻¹ (C-C), 1550-1555 cm⁻¹ (N-H), and 1615-1620 cm⁻¹ (C=C) as listed in Table 1 due to high amounts of antigens and receptor proteins presented on cancerous cell surface [12,24-26]. Nucleic acid-dominated spectra were observed by relatively strong bands of ring breathing at 680 cm⁻¹, 916 cm⁻¹, 1479-1491 cm⁻¹, and 1572-1578 cm⁻¹ because of large nuclei feature of cancer cells [24–26]. In addition, the bands at 1265 cm⁻¹ (C–H) and 1655–1680 cm⁻¹ (C=C) from phospholipid were comparatively weak because of loss in the architectural arrangement of lipid layers in cancerous cells. In contrast, healthy cells possess phospholipid-rich structure and lipid-layers in cell membrane. Therefore, the fibroblast cells (Fig. 3) showed dominant lipid-spectra at 1265 cm⁻¹ (C-C), $1350 \, \text{cm}^{-1}$ (CH/CH₂), and $1655 - 1680 \, \text{cm}^{-1}$ (C=C), as described earlier [25,30]. In addition, SERS spectrum of RBCs was investigated and specific bands were assigned as shown in Fig. 3. The spectrum was rich at wave number 754 cm⁻¹ (ring breathing), 1367 cm⁻¹ (ring stretching), and 1582-1586 cm⁻¹ (C-C), representing vibration modes of porphyrin, which is a main component of heme groups of hemoglobin [27-29,31]. It was reported that 33% of RBCs consists of hemoglobin; thus, the porphyrin-dominated spectra were observed [29]. Furthermore, other non-porphyrin bands related to components of hemoglobin protein vibrational modes were evident, such as 1175–1177 cm⁻¹ (C–H), 1440 cm⁻¹ (CH₂), 1550–1555 cm⁻¹ (N–H), and 1615-1620 cm⁻¹ (C=C), respectively. The different fingerprints between cancerous cells, fibroblasts, and RBCs make the plasmonic paper promising for cancer screening.

3.3. Detection of target cancer cells in mixture samples

Biological and clinical samples containing not only the target cancer cells but also normal cells, blood, and other biomolecules yielded complex SERS spectra resulting in complication of target cell analysis. Consequently, separation and enrichment processes are desirable to increase purity of the target and concentrate the limited amount of analytes in real samples. Magnetic separation and enrichment technique, with the advantages of ease of usage, low cost, and short processing time, have been intensively applied to capture target biomolecules to improve efficiency of detection [32]. In this study, immunomagnetic conjugates were prepared by functionalization of magnetic particles with EpCAM-specific antibody in order to recognize EpCAM-overexpressing colon cancer cells, HT-29. The conjugation was performed by carbodiimide chemistry through activation of carboxyl groups coated on magnetic beads in order to couple with amine groups of antibody. The successful conjugation was confirmed through the reduction of total negative charge of magnetic beads from -22.7 to -10.97 mV influenced by positive charge of amine groups on antibody. Prior to performing target cell enrichment in complex samples, capture efficiency of immunomagnetic conjugates was determined. The immunomagnetic conjugate was applied to capture and separate the target from a sample containing 5000 HT-29 cells spiked in PBS. After counting the enriched cells under a microscope, it was observed that the target cells were captured with high percentage above 80% demonstrating good capture efficiency. To evaluate non-specific interaction of immunomagnetic conjugates, similar amounts of non-target fibroblast

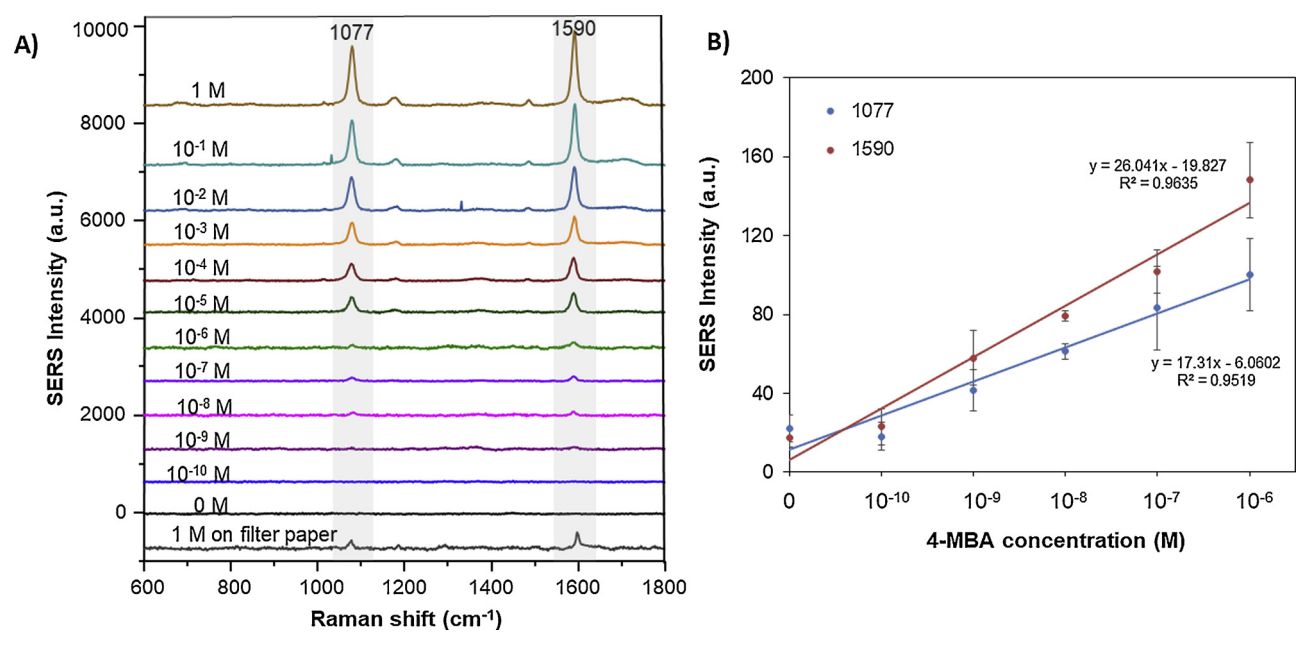


Fig. 2. Raman enhancement property of the plasmonic paper. (A) SERS spectra at different concentrations of 4-MBA obtained on the plasmonic paper. (B) Plot demonstrating the relationship of 4-MBA concentrations and SERS intensities at 1077 and 1590 cm⁻¹ on the plasmonic paper.

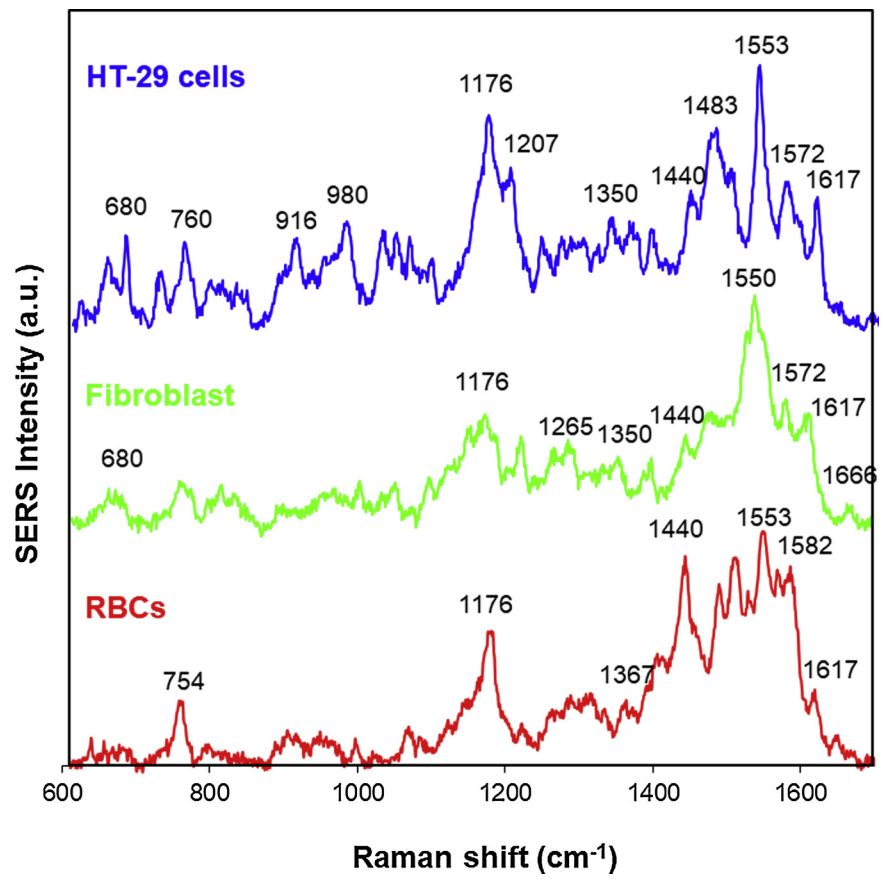


Fig. 3. SERS spectra of cancerous cells (HT-29) and non-cancerous cells (fibroblast and RBCs) on the plasmonic paper.

cells were spiked in PBS and enriched with a similar procedure independently. The result showed that less than 25% of non-target cells were captured by immunomagnetic conjugate. This result revealed that the immunomagnetic conjugate provided good affinity towards the target cells via strong and specific recognition between antibodies on the surface of the particles and EpCAM overexpressed on the target cell.

Additionally, the specific binding between immunomagnetic conjugates and target cells was much stronger than non-specific interaction due to interferences.

In order to demonstrate the detection of the target cells in biological samples that normally contain both cancer and normal cells, the target HT-29 cells were mixed with different amounts of non-target fibroblasts

Table 1
Raman peak positions and tentative vibrational mode assignment observed in this study.

Peak position ^a	Vibrational mode	Tentative assignment	References
680	Ring breathing	DNA/RNA (guanine)	[25]
754	Ring breathing	porphyrin	[27-29]
758-760	Ring breathing	Tryptophan	[24,26]
916	Ring breathing	DNA/RNA(furanose)	[26]
980	C-C stretching	β sheet	[24]
1175-1177	C-H bending	Tyrosine	[24,26]
1207-1209	C-C stretching	Phenylalanine,	[24,26]
		Tryptophan, Tyrosine	
1265	C-H deformation	lipid	[25]
1350	CH ₃ /CH ₂ twisting	lipid	[25]
1367	Half-ring stretching	porphyrin	[28]
1437-1440	CH ₂ deformation	lipid, protein	[12,24,26]
1479-1491	Ring breathing	DNA/RNA (adenine,	[26]
		guanine)	
1550-1555	N-H	Tryptophan	[12,26]
1572-1578	Ring breathing	DNA/RNA (adenine,	[24,26]
	(C-C)	guanine)	
1582-1586	C-C asymmetric	hemoglobin	[27-29,31]
	stretching		
1615-1620	C=C	Tryptophan, Tyrosine	[24,26]
1655-1680	C=C	lipid	[30]

a Approximate wavenumber range obtained in this study associating with the references.

[HT-29:fibroblast in PBS, 5000:5000 (1:1), 5000:10,000 (1:2) and 5000:25,000 (1:5)] followed by addition of $10\,\mu\text{g/mL}$ of immunomagnetic conjugates. The results showed that the cells were captured with high percentage of 84.16%, 83.20%, and 85.68%, from the mixed samples of 1:1, 1:2, and 1:5 ratios, respectively (Table S3). After target cell separation by immunomagnetic conjugates, the enriched samples from the 1:1 HT-29:fibroblast mixtures were verified through SERS spectra by dropping them on the plasmonic paper offering label-free and non-invasive detection. The average spectra of captured cells showed intense bands at 1176 cm $^{-1}$ (C–H), 1553 cm $^{-1}$ (N–H) due to large amount of protein, and strong DNA band at

1572 cm⁻¹ (C-C) corresponding to the fingerprint of HT-29 cells as demonstrated in Fig. 4A. However, shifted bands and slightly different fingerprint of the captured cells compared with that of the single HT-29 cell type were observed. The spectral deviation might derive from the captured cell suspension containing immunomagnetic conjugates (the spectrum is shown in Fig. S4) and some of fibroblast cells that were contaminated through non-specific interaction. It is not always reliable to analyze SERS spectra of complicated and heterogeneous sample by naked eyes; hence, a combination of two multivariate data analysis techniques, namely principal component analysis (PCA) and the knearest-neighbor algorithm (k-NN), was applied. PCA is widely used in spectral analysis to reduce dimension of the original data set to a few principal components (PCs) with maximized variance within a group of data. In particular, dominant spectral peaks shown in HT-29 and fibroblast including 760, 980, 1176, 1207, 1350, 1440, 1483, 1553, 1572, and 1617 cm⁻¹ as labeled in Fig. 4A were selected for analysis and PCA was used to reduce the dimension of the acquired Raman spectra to one. Fig. 4B illustrates the PCA plot from 20 samples of each group showing the relationship between spectra of single HT-29 cells (blue), single fibroblasts (green), and the captured cells (black). It can be seen that the plot of each group was clustered indicating similarity and reproducibility of SERS spectra. The resulting 1-dimensional data were then classified as either HT-29 cells or fibroblasts using the k-NN algorithm with a sensitivity of 84.8% and specificity of 82.6%, representing diverse fingerprints among cancerous and non-cancerous cells. To analyze and classify the captured cells, the spectra acquired from both the HT-29 and fibroblast were again used to construct both PCA and k-NN classifier. Then, the constructed classifier was applied to identify the captured cells as cancerous cells (HT-29) resulting in an accuracy of 83.7%.

In addition, detection of cancerous cells spiked in RBCs was demonstrated to represent the diagnosis of circulating tumor cells (CTCs) that is presented rarely in blood. Different amounts of HT-29 cells including 1000, 5000 and 10,000 cells were spiked into 0.1% RBC (approximately 4.133×10^6 cells/mL by counting) independently followed by addition of $10\,\mu\text{g/mL}$ immunomagnetic conjugates. The results demonstrated that cells were captured from the samples under

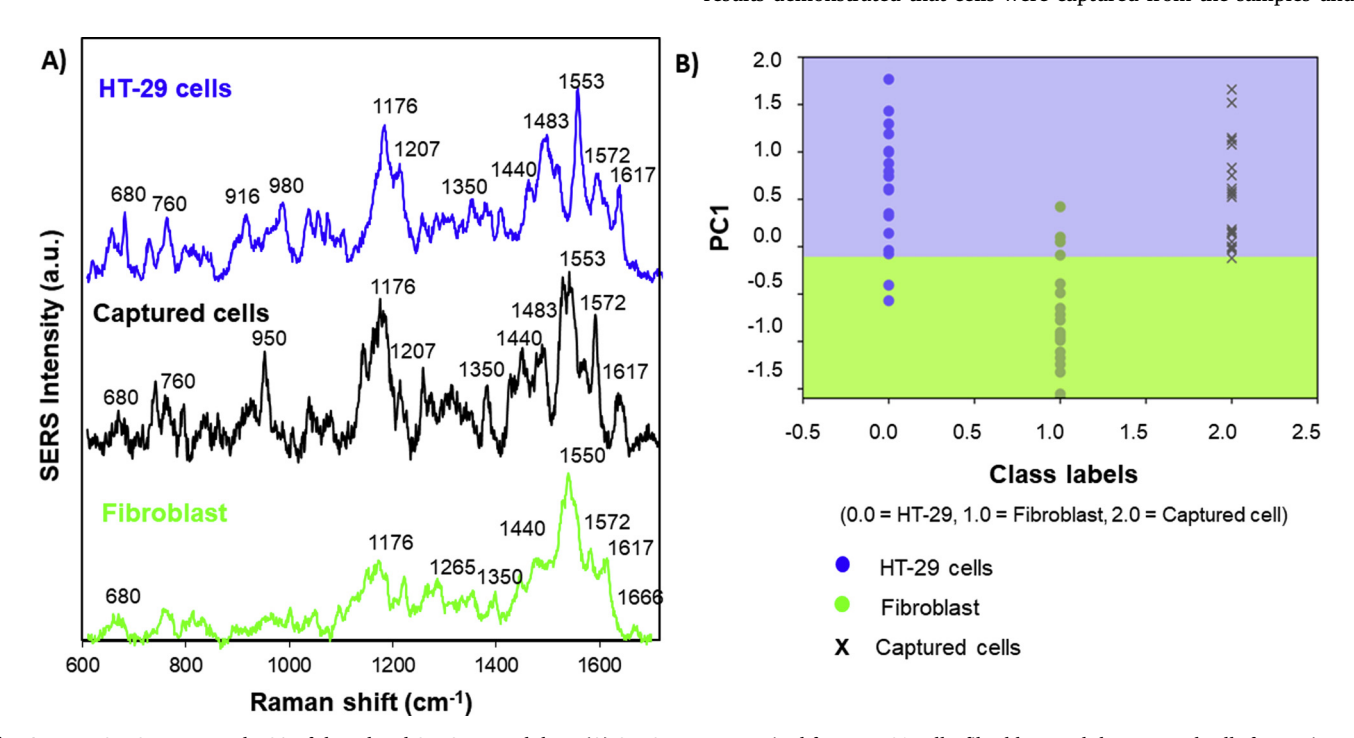


Fig. 4. Mean SERS spectra and PCA of the related SERS spectral data. (A) SERS spectra acquired from HT-29 cells, fibroblast, and the captured cells from mixtures. (B) Scatter plots of the scores from the first principal component (PC 1) of the SERS spectra from HT-29 (blue), fibroblast (green), and the captured cells (black). (For interpretation of the references to colour in this figure legend, the reader is referred to the web version of this article).

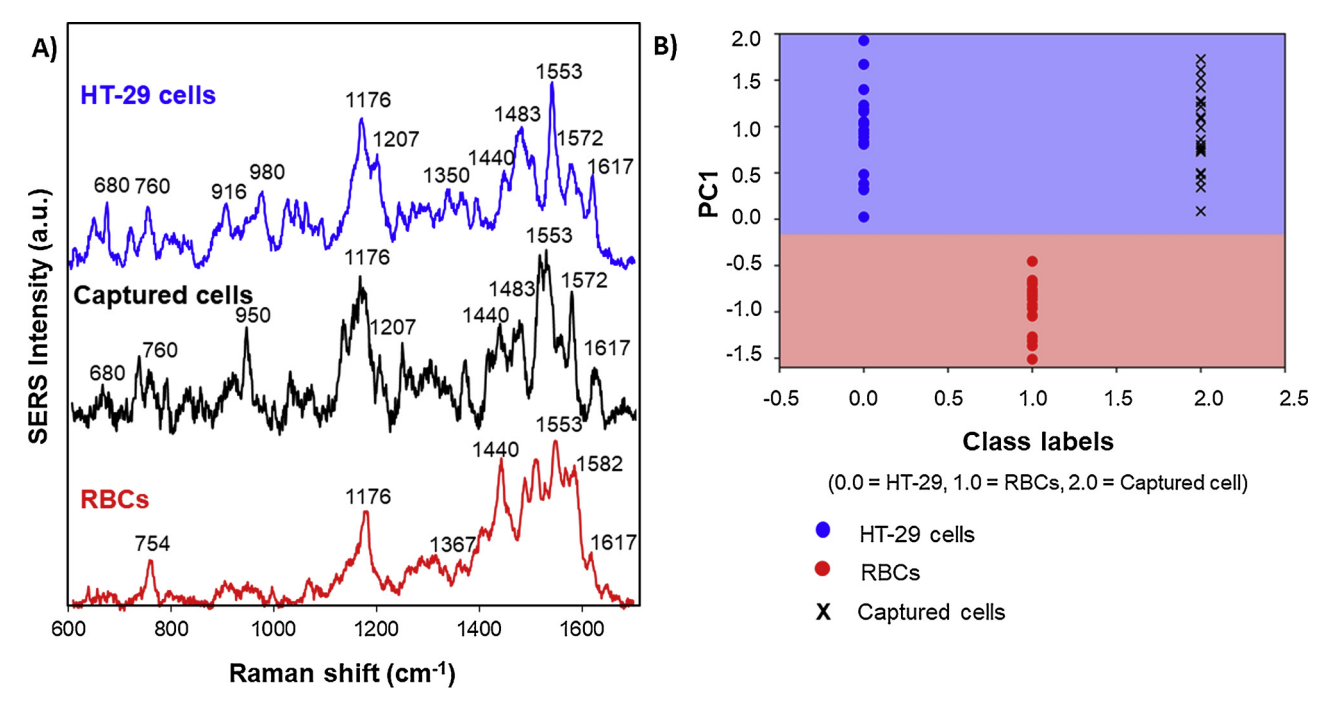


Fig. 5. Mean SERS spectra and PCA of the corresponding SERS spectral data. (A) SERS spectra obtained from HT-29 cells, RBCs, and the captured cells from mixtures. (B) Scatter plots of the scores from the first principal component (PC 1) of the SERS spectra from HT-29 (blue), RBCs (red), and the captured cells (black). (For interpretation of the references to colour in this figure legend, the reader is referred to the web version of this article).

the magnetic field with high percentage of 94.40%, 88.00%, and 83.09% from 1000, 5000, and 10,000 spiked HT-29 cells, respectively (Table S3). The results of target cell enrichment from different interferences (fibroblasts and RBCs) indicate high capture efficiency of immunomagnetic conjugates toward HT-29 cells in complex conditions. Moreover, the target cells can be simply separated from samples for further detection in less than 30 min. Fig. 5A illustrates the mean SERS spectra of the HT-29, RBCs, and the captured cells. The average SERS fingerprint of the captured cells showed strong vibrational bands of amino acid, 1176 cm⁻¹ (C-H) and 1553 cm⁻¹ (N-H), and DNA, $1572\,\mbox{cm}^{-1}$ (C–C), indicating high amount of protein and nucleic acid corresponding to cancerous cells. In addition, the bands related to porphyrin structure at 754 cm⁻¹ (ring breathing) and 1582 cm⁻¹ (C-C) were relatively weak compared with spectra of single RBC sample. The PCA analysis combined with k-NN algorithm was again performed to analyze HT-29 and RBCs SERS spectra using dominant Raman shifts including 754, 980, 1176, 1207, 1367, 1440, 1553, 1572, 1582, and 1617 cm⁻¹ as depicted in Fig. 5A. The PCA plots (Fig. 5B) calculated from characteristic peak positions of HT-29 cells and RBCs were clearly differentiated with the sensitivity of 96.4% and specificity of 100%, indicating distinctive SERS spectra between cancerous cells and RBCs. The captured cells were then identified as the cancerous cells (HT-29) with the accuracy of 98.2% using a combination of PCA and k-NN classifier similar to the previous system. Thus, we clearly demonstrated that the paper-based SERS platform with the assistance of immunomagnetic conjugates and multivariate analysis could be applied for cancer cell screening using a simple process and short time. This is comparable with other approaches that have been developed for intrinsic SERS detection of cancer. However, this platform offers significant advancement over previous platforms in minimizing complexity of SERS spectra from interferences by target cell separation process based on bio-recognition interaction between immunomagnetic conjugates and the target cells. This approach couples the sensitivity of SERS technique and specificity derived from magnetic separation that could get rid of non-target cells or other molecules contaminated in biological samples. Moreover, multivariate analysis applied in this platform facilitates the interpretation of SERS spectra and makes cancer cell identification more reliable.

4. Conclusion

A system of paper-based SERS substrate combined with magnetic separation was developed for simple and effective cancer screening. Distinguished SERS spectra of colon cancer cells, normal cells, and RBCs could be achieved, reflecting diverse levels of proteins, nucleic acids, and lipids due to structural and metabolic changes. By applying immunomagnetic conjugates, the target cells were concentrated and separated from cell mixtures with high percentage of 80-90% through specific recognition between antibodies and biomarkers overexpressed on the surface of cancer cells. Based on PCA analysis and k-NN algorithm, each cell type could be differentiated with high sensitivity and specificity. Additionally, the captured cells could be verified and identified as cancerous cells (HT-29) with high accuracy up to 98%. Our results demonstrate that the plasmonic paper with the assistance of magnetic separation and multivariate analysis provides a convenient, rapid, and cost-effective system for colon cancer cell detection, which can potentially be applied for screening other cancer cells or biomarkers.

Acknowledgements

This work was supported by a grant from Thailand Research Fund (TRF) [grant number TRG6080003] and the National Nanotechnology Center (NANOTEC), Thailand.

Appendix A. Supplementary data

Supplementary material related to this article can be found, in the online version, at doi:https://doi.org/10.1016/j.snb.2019.01.090.

References

 M. Perfe'zou, A. Turner, A. Merkoçi, Cancer detection using nanoparticle-based sensors, Chem. Soc. Rev. 41 (2012) 2606–2622, https://doi.org/10.1039/

- c1cs15134g.
- [2] W.E. Doering, M.E. Piotti, M.J. Natan, R.G. Freeman, SERS as a foundation for nanoscale, optically detected biological labels, Adv. Mater. 19 (2007) 3100–3108, https://doi.org/10.1002/adma.200701984.
- [3] M.E. Stewart, C.R. Anderton, L.B. Thompson, J. Maria, S.K. Gray, J.A. Rogers, R.G. Nuzzo, Nanostructured plasmonic sensors, Chem. Rev. 108 (2008) 494–521, https://doi.org/10.1021/cr068126n.
- [4] M.J. Banholzer, J.E. Millstone, L. Qin, C.A. Mirkin, Rationally designed nanostructures for surface enhanced Raman spectroscopy, Chem. Soc. Rev. 37 (2008) 885–897, https://doi.org/10.1039/b710915f.
- [5] M.J. Oliveira, P. Quaresma, M. Peixoto de Almeida, A. Araujo, E. Pereira, E. Fortunato, R. Martins, R. Franco, H. Águas, Office paper decorated with silver nanostars - an alternative cost effective platform for trace analyte detection by SERS, Sci. Rep. 7 (2017) 2480, https://doi.org/10.1038/s41598-017-02484-8.
- [6] Y. Li, K. Zhang, J. Zhao, J. Ji, C. Ji, B. Liu, A three-dimensional silver nanoparticles decorated plasmonic paper strip for SERS detection of low-abundance molecules, Talanta 147 (2016) 493–500, https://doi.org/10.1016/j.talanta.2015.10.025.
- [7] M.N. Costa, B. Veigas, J.M. Jacob, D.S. Santos, J. Gomes, P.V. Baptista, R. Martins, J. Inácio, E. Fortunato, A low cost, safe, disposable, rapid and self-sustainable paper-based platform for diagnostic testing: lab-on-paper, Nanotechnology 25 (2014) 94006, https://doi.org/10.1088/0957-4484/25/9/094006.
- [8] W.W. Yu, I.M. White, Inkjet-printed paper-based SERS dipsticks and swabs for trace chemical detection, Analyst 138 (2013) 1020–1025, https://doi.org/10.1039/ c2an36116g.
- [9] J. Wang, L. Yang, B. Liu, H. Jiang, R. Liu, J. Yang, G. Han, Q. Mei, Z. Zhang, Inkjet-printed silver nanoparticle paper detects airborne species from crystalline explosives and their ultratrace residues in open environment, Anal. Chem. 86 (2014) 3338–3345, https://doi.org/10.1021/ac403409q.
- [10] Y. Zhu, M. Li, D. Yu, L. Yang, A novel paper rag as 'D-SERS' substrate for detection of pesticide residues at various peels, Talanta 128 (2014) 117–124, https://doi.org/ 10.1016/j.talanta.2014.04.066.
- [11] W. Kim, Y.H. Kim, H.K. Park, S. Choi, Facile fabrication of a silver nanoparticle immersed, surface-enhanced Raman scattering imposed paper platform through successive ionic layer absorption and reaction for on-site bioassays, ACS Appl. Mater. Interfaces 7 (2015) 27910–27917, https://doi.org/10.1021/acsami. 5h09982
- [12] Q. Liu, J. Wang, B. Wang, Z. Li, H. Huang, C. Li, X. Yu, P.K. Chu, Paper-based plasmonic platform for sensitive, noninvasive, and rapid cancer screening, Biosens. Bioelectron. 54 (2014) 128–134, https://doi.org/10.1016/j.bios.2013.10.067.
- [13] B. Nikoobakht, M.A. El-Sayed, Preparation and growth mechanism of gold nanorods (NRs) using seed-mediated growth method, Chem. Mater. 15 (2003) 1957–1962, https://doi.org/10.1021/cm020732l.
- [14] S. Bamrungsap, A. Treetong, C. Apiwat, T. Wuttikhun, T. Dharakul, SERS-fluorescence dual mode nanotags for cervical cancer detection using aptamers conjugated to gold-silver nanorods, Microchim. Acta 183 (2016) 249–256, https://doi.org/10.1007/s00604-015-1639-9.
- [15] C.H. Lee, L. Tian, S. Singamaneni, Paper-based SERS swab for rapid trace detection on real-world surfaces, ACS Appl. Mater. Interfaces 2 (2010) 3429–3435, https://doi.org/10.1021/am1009875.
- [16] C.H. Lee, M.E. Hankus, L. Tian, P.M. Pellegrino, S. Singamaneni, Highly sensitive surface enhanced Raman scattering substrates based on filter paper loaded with plasmonic nanostructures, Anal. Chem. 83 (2011) 8953–8958, https://doi.org/10. 1021/ac2016882.
- [17] E. Satheeshkumar, P. Karuppaiya, K. Sivashanmugan, W.T. Chao, H.S. Tsay,

- M. Yoshimura, Biocompatible 3D SERS substrate for trace detection of amino acids and melamine, Spectrochim. Acta A Mol. Biomol. Spectrosc. 181 (2017) 91–97, https://doi.org/10.1016/j.saa.2017.03.040.
- [18] S.K. Ghosh, T. Pal, Interparticle coupling effect on the surface plasmon resonance of gold nanoparticles: from theory to applications, Chem. Rev. 107 (2007) 4797–4862, https://doi.org/10.1021/cr0680282.
- [19] K.L. Kelly, E. Coronado, L.L. Zhao, G.C. Schatz, The optical properties of metal nanoparticles: the influence of size, shape, and dielectric environment, J. Phys. Chem. B 107 (2003) 668–677, https://doi.org/10.1021/jp026731y.
- [20] S. Zhu, C. Fan, J. Wang, J. He, E. Liang, Surface-enhanced Raman scattering of 4-mercaptobenzoic acid and hemoglobin adsorbed on self-assembled Ag monolayer films with different shapes, Appl. Phys. A 117 (2014) 1076–1083, https://doi.org/10.1007/s00339-014-8548-3.
- [21] W.S. Kim, J.H. Shin, H.K. Park, S. Choi, A low-cost, monometallic, surface-enhanced Raman scattering-functionalized paper platform for spot-on bioassays, Sens. Actuators B Chem. 222 (2016) 1112–1118, https://doi.org/10.1016/j.snb.2015.08.
- [22] W.L.J. Hasi, S. Lin, X. Lin, X.T. Lou, F. Yang, D.Y. Lin, Z.W. Lu, Rapid fabrication of self-assembled interfacial film decorated filter paper as an excellent surface-enhanced Raman scattering substrate, Anal. Methods 24 (2014) 9547–9553, https:// doi.org/10.1039/C4AY01775G.
- [23] M. Hou, Y. Huang, L. Ma, Z. Zhang, Quantitative analysis of single and mix food antiseptics basing on SERS spectra with PLSR method, Nanoscale Res. Lett. 11 (2016) 296, https://doi.org/10.1186/s11671-016-1507-5.
- [24] I. Notingher, L.L. Hench, Raman microspectroscopy: a noninvasive tool for studies of individual living cells in vitro, Exp. Rev. Med. Devices 3 (2006) 215–234, https://doi.org/10.1586/17434440.3.2.215.
- [25] C.M. Girish, S. Iyer, K. Thankappan, V.V.D. Rani, G.S. Gowd, D. Menon, S. Nair, M. Koyakutty, Rapid detection of oral cancer using Ag-TiO2 nanostructured surface-enhanced Raman spectroscopic substrates, J. Mater. Chem. B 2 (2014) 989–998, https://doi.org/10.1039/C3TB21398F.
- [26] A.C. Terentis, S.A. Fox, S.J. Friedman, E.S. Spencer, Confocal Raman microspectroscopy discriminates live human metastatic melanoma and skin fibroblast cells, J. Raman Spectrosc. 44 (2013) 1205–1216, https://doi.org/10.1002/jrs.4363.
- [27] W.R. Premasiri, J.C. Lee, L.D. Ziegler, Surface-enhanced Raman scattering of whole human blood, blood plasma, and red blood cells: cellular processes and bioanalytical sensing, J. Phys. Chem. B 116 (2012) 9376–9386, https://doi.org/10.1021/ ip304932g.
- [28] J. Shao, H. Yao, L. Meng, Y. Li, M. Lin, X. Li, J. Liu, J. Liang, Raman spectroscopy of circulating single red blood cells in microvessels in vivo, Vib. Spectrosc. 63 (2012) 367–370, https://doi.org/10.1016/j.vibspec.2012.08.004.
- [29] S. Zhang, X. Tian, J. Yin, Y. Liu, Z. Dong, J.L. Sun, W. Ma, Rapid, controllable growth of silver nanostructured surface-enhanced Raman scattering substrates for red blood cell detection, Sci. Rep. 6 (2016) 24503, https://doi.org/10.1038/ srep24503.
- [30] M. Votteler, D.A.C. Berrio, M. Pudlas, H. Walles, K. Schenke-Layland, Non-contact, label-free monitoring of cells and extracellular matrix using Raman spectroscopy, J. Vis. Exp. 63 (2012) e3977, https://doi.org/10.3791/3977.
- [31] Y.Y. Huang, N. Li, S.N. Zhou, Z.T. Huang, Z.F. Zhuang, Study of hemoglobin response to mid-ultraviolet (UVB) radiation using micro-Raman spectroscopy, Appl. Phys. B 123 (2017) 237, https://doi.org/10.1007/s00340-017-6800-1.
- [32] I. Safarik, M. Safarikova, Magnetic techniques for the isolation and purification of proteins and peptides, Biomagn. Res. Technol. 2 (2004) 7, https://doi.org/10. 1186/1477-044X-2-7.